

1 A FIELD VALIDATED SURROGATE CROP MODEL FOR
2 PREDICTING ROOTZONE MOISTURE AND SALT CONTENT IN
3 REGIONS WITH SHALLOW GROUNDWATER

4 Zhongyi Liu¹, Zailin Huo^{1*}, Chaozi Wang¹, Limin Zhang², Xianghao Wang¹,
5 Guanhua Huang¹, Xu Xu¹, Tammo S. Steenhuis^{3*}

6
7 1. Center for Agricultural Water Research in China, China Agricultural University, Beijing,
8 100083, PR China

9 2. School of Water Resources and Environment, China University of Geosciences, Beijing,
10 100083, PR, China

11 3. Department of Biological and Environmental Engineering, Cornell University, Ithaca, NY,
12 USA.

13
14 Correspondence to: Zailin Huo (huozl@cau.edu.cn)

15 Tammo S. Steenhuis (tss1@cornell.edu)

16
17
18
19
20
21

22 **Abstract**

23 Optimum performance of irrigated crops in regions with shallow saline groundwater
24 requires a careful balance between application of irrigation water and upward
25 movement of salinity from the groundwater. Few field validated surrogate models are
26 available to aid in the management of irrigation water under shallow groundwater
27 conditions. The objective of this research is to develop a model that can aid in the
28 management using a minimum of input data that is field validated. In this paper a
29 2-year field experiment was carried out in the Hetao irrigation district in Inner
30 Mongolia, China and a physically based integrated surrogate model for arid irrigated
31 areas with shallow groundwater was developed and validated with the collected field
32 data. The integrated model that links crop growth with available water and salinity in
33 the vadose zone is called Evaluation of the Performance of Irrigated Crops and Soils
34 (EPICS). EPICS recognizes that field capacity is reached when the matric potential is
35 equal to the height above the groundwater table and thus not by a limiting hydraulic
36 conductivity. In the field experiment, soil moisture contents and soil salt conductivity
37 at 5 depths in the top 100 cm, groundwater depth, crop height, and leaf area index
38 were measured in 2017 and 2018. The field results were used for calibration and
39 validation of EPICS. Simulated and observed data fitted generally well during both
40 calibration and validation. The EPICS model that can predict crop growth, soil water,
41 groundwater depth and soil salinity can aid in optimizing water management in
42 irrigation districts with shallow aquifers.

43 **Key words:** Surrogate hydrological model, irrigated crops, shallow aquifer

Nomenclature			
ET ₀	Reference evapotranspiration (mm)	p	Fraction of readily available soil water relative to the total available soil water
ET _P	Potential evapotranspiration (mm)	S	Salt stress coefficient ()
E _p	Potential evaporation (mm)	B	Crop specific parameter (%)
T _p	Potential transpiration (mm)	k _y	Factor that affects crop yield
E _a	Actual evaporation (mm)	E _{Ce}	Electrical conductivity of the soil saturation extract (mS cm ⁻¹)
T _a	Actual transpiration (mm)	EC _{threshold}	Threshold of the electrical conductivity of the soil saturation extract when the crop yield becomes affected by salt (mS cm ⁻¹)
K _c	Crop coefficient()	EC _{1:5}	Electrical conductivity of the soil extract that soil samples mixed with distilled water in a proportion of 1:5 (mS cm ⁻¹)
τ	Development stage of the leaf canopy()	θ _s	Soil moisture content at saturation (cm ⁻³ cm ⁻³)
r _τ	Root function for transpiration ()	φ _b	Bubbling pressure (cm)
r _E	Root function for transpiration ()	φ _m	Matric potential (cm)
j	Number of soil layer()	λ	Pore size distribution index
LAI	Leaf area index()	h	Groundwater depth (cm)
T _{mean}	Mean daily temperature (°C)	z	Depth of the point below the soil surface (cm)
T _{mx}	Maximum daily temperature (°C)	W _{fc} (h)	Total water content at field capacity of the soil profile over a prescribed depth (cm)
T _{mn}	Minimum daily temperature (°C)	L(j)	Height of layer j (cm)
LAI _{mx}	Maximum leaf area index	μ	Drainable porosity
RD _{mx}	Maximum root depth (cm)	P	Precipitation (mm)
K _b	Dimensionless canopy extinction coefficient	I	Irrigation (mm)
PHU	Total potential heat units required for crop maturation (°C)	n	Number of soil layers
Z _{1j}	Depth of the upper boundaries of soil layer j (cm)	R _{gw}	Percolation to groundwater (mm)
Z _{2j}	Depth of the lower boundaries of the soil layer for r _E (j,t); root depth or the lower boundaries of the soil layer for r _τ (j,t) (cm)	R _w (j-1,t)	Percolation rate to layer j from layer j-1 at day t (mm)
δ	Water use distribution parameter	C(j,t)	Salt concentration of layer j at day t (g L ⁻¹)
k _E	Water stress coefficient for evaporation	C _i	Salt concentration of irrigation water (g L ⁻¹)
k _τ	Water stress coefficient for transpiration	C _{gw}	Salt concentration of groundwater (g L ⁻¹)
θ	Soil moisture content (cm ⁻³ cm ⁻³)	U _{gw}	Actual upward flux of groundwater (mm)
θ _{fc}	Soil moisture content at field capacity (cm ⁻³ cm ⁻³)	U _{gw,max}	Maximum upward flux of groundwater (mm)
θ _r	Soil moisture content at wilting point (cm ⁻³ cm ⁻³)	a	Constant used for calculation of U _{gw,max} ()
f _{shape}	Shape factor of kT curve ()	b	Constant used for calculation of U _{gw,max} ()

45 **1. Introduction**

46 Irrigation water is a scarce resource, especially in arid and semi-arid areas of the
47 world. Irrigation improves quality and quantity of food production; however, excess
48 irrigation and salinization remain one of the key challenges. Almost 20% of the
49 irrigated land in the world is affected by salinization and this percentage is still on the
50 rise (Li et al., 2014). Salinity affects agricultural production (Williams, 1999). Soil
51 salinization and water shortages, especially associated with surface irrigated
52 agriculture in arid to semi-arid areas, is a threat to the well-being of local communities
53 in these areas (Dehaan and Taylor, 2002; Rengasamy, 2006).

54 In arid and semi-arid surface irrigation [with flood irrigation and](#) districts without a
55 drainage infrastructure, the groundwater table is close to the surface because more
56 water has been applied than crop evapotranspiration. Capillary rise of the shallow
57 groundwater can be used to supplement irrigation and thereby, in closed basins, can
58 possibly save water for irrigating additional areas downstream (Gao et al., 2015; Yeh
59 and Famiglietti, 2009; Luo and Sophocleous, 2010.). However, at the same time,
60 capillary upward moving water carries salt from the groundwater increasing the salt in
61 the upper layers of the soil leading to soil degradation and possibly decreasing yields
62 and change of crop patterns to more salt tolerant crops (Guo et al., 2018; Huang et al.,
63 2018). [The leaching of salts with irrigation water is necessary and useful for irrigated](#)
64 [agriculture \(Letey et al., 2011\). In north China, the fields are commonly irrigated in the](#)
65 [autumn before soil freezing to leach salts and provide water for first growth after](#)
66 [deeding in the following year \(Feng et al., 2005; Pereira et al., 2007\).](#)

67 Tradeoffs between irrigation practices and soil salinity were studied by a lot of
68 researchers (Hanson et al., 2008; Pereira et al., 2002, 2009; Minhas et al., 2020).
69 Minhas et al. (2020) give a brief review of crop evapotranspiration and water
70 management issues when coping with salinity in irrigated agriculture. Phogat et al.
71 (2020) assessed the effects of long-term irrigation on salt build-up in the soil under
72 unheated greenhouse conditions by the UNSA-TCHEM and HYDRUS-1D (Phogat et
73 al., 2020).

74 Therefore, understanding the interaction of improved crop yield, soil salinization
75 and decreased surface irrigation is important to the sustainability of the surface
76 irrigation water systems in arid and semi-arid areas. This will require experimentation
77 under realistic farmers' field conditions, as well as modeling to extend the findings
78 beyond the plot scale.

79 Field scale models for water, solute transport and crop growth are widely
80 available. Crop growth models use either empirical functions or model the underlying
81 physiological processes (Liu, 2009). Models widely used for simulating crop growth
82 are EPIC (Williams et al., 1989), DSSAT (Uehara, 1989), WOFOST (Diepen et al.,
83 1989) and AquaCrop (Hsiao et al., 2009; Raes et al., 2009; Steduto et al., 2009).
84 Models focused on water and solute movement in the vadose zone using some form
85 of Richards' equation are HYDRUS (Šimůnek et al., 1998) and SWAP (Dam et al.,
86 1997). Models that integrate crop growth and water-solute movement processes are
87 SWAP-WOFOST (Hu et al., 2019), SWAP-EPIC (Xu et al., 2015; Xu et al., 2016),
88 HYDRUS-EPIC ((Wang et al., 2015), and HYDRUS-DSSAT (Shelia et al., 2018).

89 These integrated models require input data that are usually not available when
90 applied over extended areas (Liu et al., 2009; Xu et al., 2016; Hu et al., 2019). The
91 EPIC crop growth model is often preferred in integrated crop growth hydrology
92 models because it requires relatively few input data and is accurate (Wang et al.,
93 2014; Xu et al., 2013; Chen et al., 2019).

94 There is a tendency with the advancement of computer technology to include
95 more physical processes in these models (Asher et al., 2015; Doherty and Simmons,
96 2013; Leube et al., 2012). Detailed spatially input of soil hydrological properties and
97 crop growth are required to take advantage of the model complexity (Flint et al., 2002;
98 Rosa et al., 2012). This greater model complexity, both in space and time, requires
99 longer model run times, especially for the time-dependent models (Leube et al., 2012).
100 These models are useful for research purposes but for actual field applications, the
101 required input data are not available and expensive to obtain. In such cases, simpler
102 surrogate models are a good alternative (Blanning, 1975; Willcox and Péraire, 2002;
103 Regis and Shoemaker, 2005). Surrogate models run faster and are as accurate as
104 the complex models for a specific problem (shallow groundwater here) but not as
105 versatile as the more complex models that can be applied over a wide range of
106 conditions (Asher et al., 2015).

107 Simple surrogate models are abundant in China for areas where the groundwater
108 is deeper than approximately 10 m (Kendy et al., 2003; Chen et al., 2010; Ma et al.,
109 2013; Li et al., 2017; [Wu et al., 2016](#)), but are limited and relatively scarce for areas
110 where the groundwater is near the surface in the arid to semi-arid areas (Xue et al.,

111 2018; Gao et al., 2017; Liu et al., 2019). In these areas with shallow aquifer, the
112 upward groundwater flux from groundwater is an important factor in meeting the
113 evapotranspiration demand of the crop (Babajimopoulos et al., 2007; Yeh and
114 Famiglietti, 2009). The advantage of applying surrogate models in areas with shallow
115 aquifer is that they can simulate the hydrological process with fewer parameters using
116 with simpler and computationally less demanding mathematical relationships than the
117 traditional finite element or difference models (Wu et al., 2016; Razavi et al., 2012).

118 The change in matric potential is often ignored in these surrogate models for
119 soils with a deep groundwater table. However, for areas with shallow aquifers (i.e.,
120 less than approximately 3 m), the matric potential cannot be ignored. The flow of
121 water is upward when the absolute value of matric potential is greater than the
122 groundwater depth or downward when it is less than the groundwater depth (Gardner,
123 1958; Gardner et al., 1970a; b; Steenhuis et al., 1988). The field capacity in these
124 soils is reached when the hydraulic gradient is constant (i.e., the constant value of
125 sum of matric potential and gravity potential). In this case, the soil water is in
126 equilibrium and no flow occurs.

127 Xue et al. (2018) and Gao et al. (2017), developed models for the shallow
128 groundwater, but used field capacities and drainable porosities that were calibrated
129 and independent of the depth of the groundwater. This is inexact when the
130 groundwater is close to the surface. Liu et al. (2019), used for simulating shallow
131 groundwater the same type of model as described in this paper but calibrated crop
132 evaporation and did not simulate the salt concentrations in the soil. This made their

133 model less useful for practical application.

134 Because of the shortcomings in the above complex models, we avoided the use
135 of a constant drainable porosity and considered the crop growth and thus improved
136 the surrogate model in our last study (Liu et al., 2019). The objective of this research
137 was to develop a field validated surrogate model that could be used to simulate the
138 water and salt movement and crop growth in irrigated areas with shallow groundwater
139 and salinized soil with a minimum of input parameters. To validate the surrogate
140 model, we performed a 2-year field experiment in the Hetao irrigation district that
141 investigated the change in soil salinity, moisture content, groundwater depth and
142 maize and sunflower growth during the growing season.

143 In the following section we present first the theoretical background of the
144 surrogate model. The model consists of crop growth module and a vadose zone
145 module. This is followed by detailed description of the two-year field experiments
146 starting in 2017 in the Hetao irrigation district where maize and sunflower were
147 irrigated by flooding the field. The experimental results consisting of climate data,
148 irrigation application, crop growth parameters, moisture and salt content and
149 groundwater depth are used to calibrate and validate the model.

150 **2. Model description**

151 2.1 Introduction of the model

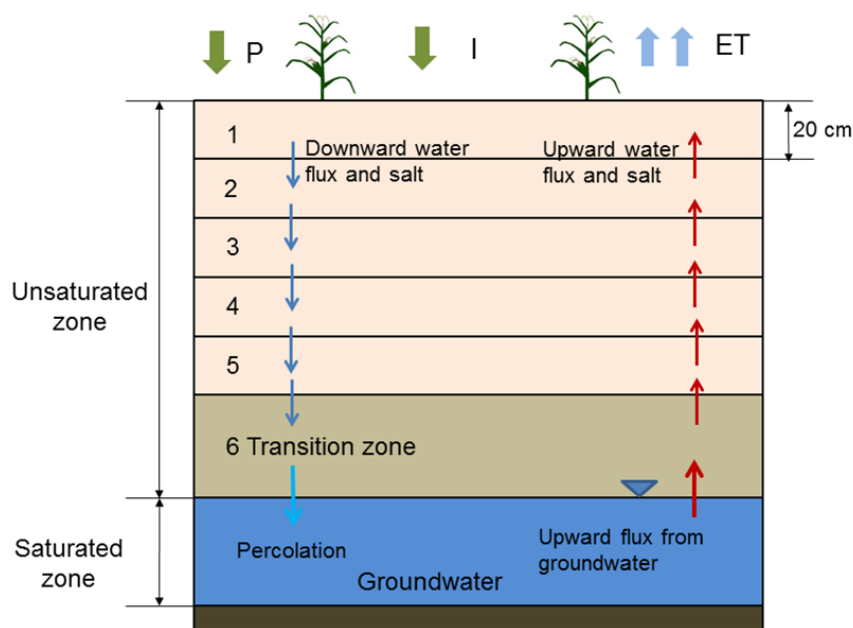
152 In a recent study, we presented a surrogate model for the vadose zone with shallow
153 groundwater using the novel concept that the moisture content at field capacity is a
154 unique function of the groundwater depth after irrigation or precipitation that wets up

155 the entire soil profile. The model, called the Shallow Vadose Groundwater model,
 156 applies directly to surface irrigated districts where the groundwater is within 3.3 m
 157 from the soil surface (Liu et al. 2019). The model was a proof of concept with
 158 calibrated values for evapotranspiration and soil salinity and was not simulated.

159 To make the Shallow Vadose Groundwater model more physically realistic, we
 160 added a crop growth model and included the effect of salinity and moisture content on
 161 evaporation and transpiration directly in this study. The new model that combines
 162 parts of the Environmental Policy Integrated Climate (EPIC) with Shallow Vadose
 163 Groundwater model is called the *Evaluation of the Performance of Irrigated Crops*
 164 *and Soils* (EPICS).

165 2.2 Structure of the EPICS model

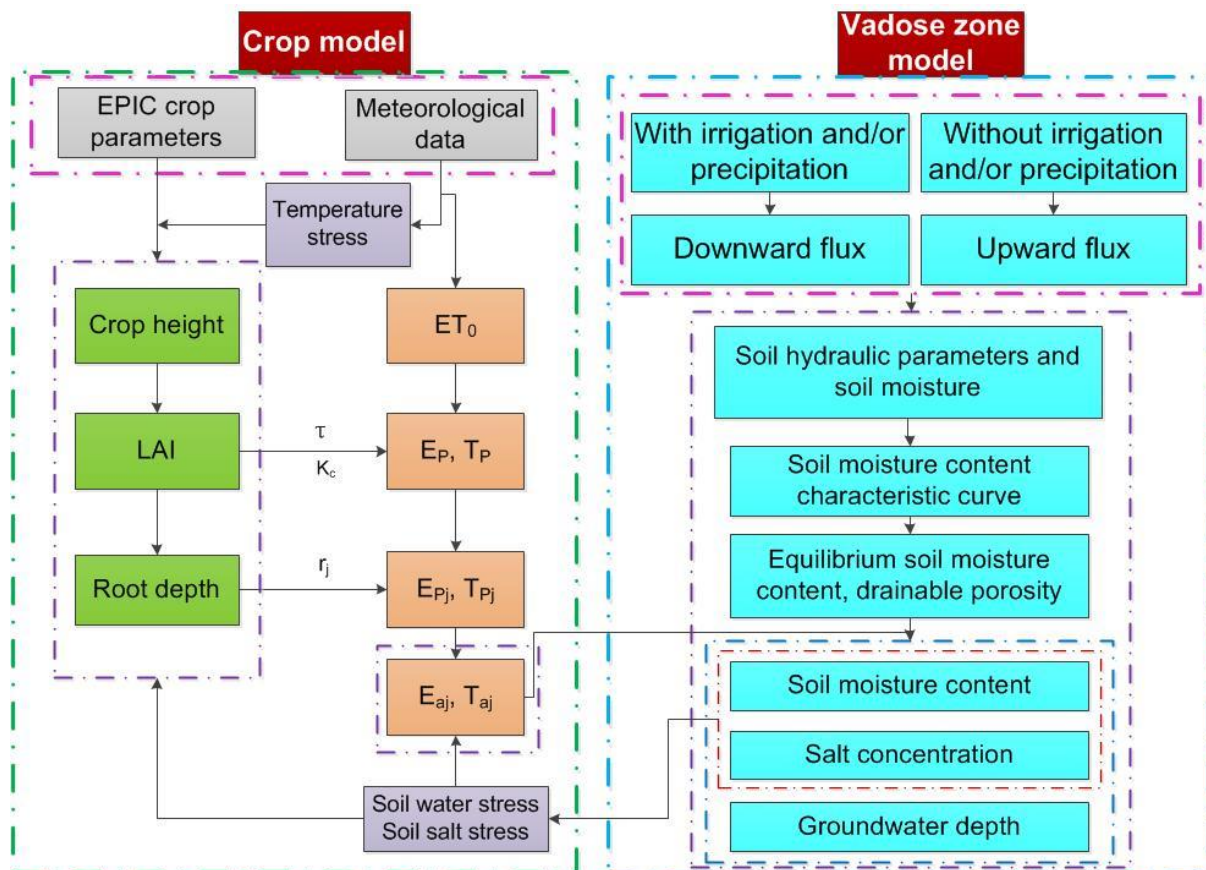
166 In the EPICS model, the soil profile is divided into five layers of 20 cm (from the soil
 167 surface down) and a sixth layer that stretches from the 100 cm depth to the water
 168 table below (Fig. 1).



170 Fig 1. Schematic diagram of model components and water movement

171 The moisture content and salt content are calculated for each day (Fig.1). All flow
172 takes place within the day and the water and salt content are in “equilibrium” (i.e.,
173 fluxes are zero) at the end of the day for which the calculations are made. Daily fluxes
174 considered in the vadose model are the following: at the surface, the fluxes are
175 irrigation, both irrigation water, $I(t)$, and salt, $S_o(t)$, and precipitation, $P(t)$, and for each
176 layer, j , on days with irrigation and rainfall, the downward flux of water, $R_w(j,t)$, and salt,
177 $S(j,t)$, between the layers. On days without water input at the soil surface, an upward
178 groundwater flux $U(j,h,t)$, and salt, $S(j,t)$ are considered. The flux to the surface
179 depends on the groundwater depth. Finally, transpiration, $T(j,t)$, removes water from
180 the layers with roots of the crops and evaporation, $E(j,t)$, from all layers.

181 The EPICS model consists of two modules: the VADOSE module and the CROP
182 module. The two modules are linked through the evapotranspiration flux in the soil
183 (Fig. 2).



184

185 Fig 2. Schematic diagram of the linked novel Shallow Aquifer-Vadose zone surrogate
 186 module and EPIC module. Note: ET_0 is the reference evapotranspiration, E_p and T_p
 187 are the potential evaporation and potential transpiration, E_a and T_a are the actual
 188 evaporation and actual transpiration, K_c is the crop coefficient, τ is the development
 189 stage of the leaf canopy, and r_j is the root function of soil layer j .

190

191 The CROP module employs functions of the EPIC model (Williams et al., 1989)
 192 and root growth distribution (Novak, 1987; Kendy et al., 2003; Chen et al. 2019). The
 193 CROP module calculates daily values of crop height, root depth and leaf area index
 194 (LAI) based on climatic data (Fig. 2).

195 The VADOSE module calculates the moisture and salt content in the root zone
 196 and the upward movement of the groundwater (Fig.2). Field capacity varies with
 197 depth and is a function of the (shallow) groundwater depth and the soil characteristic
 198 curve (Liu et al., 2019). Moisture contents become less than field capacity when the

199 upward flux is less than the actual evapotranspiration.

200 Finally, the link between the VADOSE and the CROP modules is achieved by
201 calculating the actual evapotranspiration with parameters of both modules consisting
202 of the moisture content and the salt content simulated in the VADOSE module and
203 root distribution and potential evapotranspiration in the CROP module (Fig. 2).

204 2.3 Theoretical background of the EPICS model

205 In the next section, the equations of the CROP in the VADOSE modules are
206 presented. The calculations are carried out sequentially on a daily time step. [This](#)
207 [model predicts field daily soil water, salt content and crop growth, which are critical](#)
208 [parameters for irrigation water management. For field and regional water](#)
209 [management and irrigation policy development, resolution of daily time step is](#)
210 [sufficient.](#) Finer resolution is not needed for managing water and salt content for
211 irrigation. In the first step, the actual evaporation and transpiration are calculated for
212 each layer in the model. Next, the moisture content and salt content are adjusted for
213 the various fluxes. Since the equations for the downward movement on days of
214 rainfall and/or irrigation are different than for upward movement from the groundwater
215 on the remaining days, we present upward and downward movement in separate
216 sections. The code was written in Matlab 2014Ra and Microsoft Excel was used for
217 data input and output.

218 2.3.1 CROP module

219 The crop module uses functions of EPIC (Erosion Productivity Impact Calculator,

220 Williams et al., 1989) to calculate leaf area index, LAI, crop height and the root depth
 221 (green boxes in Fig. 2), and the potential transpiration, T , and evaporation, E (orange
 222 boxes in Fig, 2). Input data for the CROP module included: mean daily temperature
 223 (T_{mean}), maximum daily temperature (T_{mx}), minimum daily temperature (T_{mn}),
 224 maximum crop height (H_{mx}), maximum LAI (LAI_{mx}), maximum root depth (RD_{mx}),
 225 dimensionless canopy extinction coefficient (K_b), and total potential heat units
 226 required for crop maturation (PHU).

227 The potential rates of evaporation, $E_p(j, t)$, and transpiration, $T_p(j, t)$, of different
 228 layers are derived from the total rates and a root function that determines the
 229 distribution of roots in the vadose zone

$$T_p(j, t) = r_T(j, t)T_p(t) \quad (1a)$$

$$E_p(j, t) = r_E(j, t)E_p(t) \quad (1b)$$

231 where j is the number of soil layers and t is the day number, $T_p(t)$ is the total
 232 potential transpiration and $E_p(t)$ is the total potential transpiration at time, t . Both are
 233 calculated with the CROP module (S1 in the supplementary material). Root functions
 234 (Sau et al., 2004; Delonge et al., 2012) were used to calculate transpiration and
 235 evaporation of different soil layer. $r_T(j, t)$ is the root function for the transpiration and
 236 $r_E(j, t)$ is the root function for the evaporation. Both have the same general equation
 237 but with a different value for the constant δ .

$$r_T(j, t) = \left[\frac{1}{1 - \exp(-\delta)} \right] \left\{ \exp \left[-\delta \left(\frac{Z_{1j}}{Z_{2j}} \right) \right] \left[1 - \exp \left(-\delta \frac{Z_{2j} - Z_{1j}}{Z_r} \right) \right] \right\} \quad (2a)$$

$$r_E(j, t) = \left[\frac{1}{1 - \exp(-\delta)} \right] \left\{ \exp \left[-\delta \left(\frac{Z_{1j}}{Z_{2j}} \right) \right] \left[1 - \exp \left(-\delta \frac{Z_{2j} - Z_{1j}}{Z_r} \right) \right] \right\} \quad (2b)$$

238 Where z_{1j} is the depth of the upper boundaries of the soil layer j . For $r_T(j, t)$ if the
 239 root depth is smaller than the lower boundaries of the soil layer j , Z_{2j} is equal to the
 240 root depth and if the root depth is greater than the lower boundaries of the soil layer j ,
 241 Z_{2j} is the depth of the lower boundaries of the soil layer j . For $r_E(j, t)$, Z_{2j} is depth of
 242 the lower boundaries of the soil layer j . Z_r is the root zone depth and δ is the water
 243 use distribution parameter. Note that the sum of $r_T(j, t)$ of all soil layers is equal to 1.
 244 In the study of Novark (1987), the value of δ for corn is 3.64 and we used this value.
 245 To obtain $r_E(j, t)$, δ was set to 10 (Chen et al., 2019; Kendy et al., 2003). Sunflower
 246 root function simulation employed the same δ values as for maize.

247 The actual evaporation rates, $E_a(j, t)$, and transpiration, $T_a(j, t)$, for each soil
 248 layer, j , at time, t , are calculated as a proportion of the potential values as:

$$E_a(j, t) = k_E(j, t)E_p(j, t) \quad (3a)$$

$$T_a(j, t) = k_T(j, t)S(j, t)T_p(j, t) \quad (3b)$$

250 where $k_E(j)$ and $k_T(j)$ are water stress coefficients and $S(j)$ is a salt stress
 251 coefficient. According to Raes et al. (2009), the water stress coefficients are

$$k_E(j, t) = \exp\left(-2.5 \frac{\theta_{fc}(j) - \theta(j, t)}{\theta_{fc}(j) - \theta_r(j)}\right) \quad \theta \leq \theta_{fc} \quad (4a)$$

$$k_E(j, t) = 1 \quad \theta > \theta_{fc} \quad (4b)$$

253 where $\theta_{fc}(j)$ is the moisture content at [field capacity](#) for layer j , or when the
 254 conductivity becomes limiting and $\theta_r(j)$ is the moisture content at wilting point,
 255 $\theta(j, t)$ is the soil moisture content for layer j at time t .

256 Then water stress coefficient in Eq. 3b is:

$$k_T(j, t) = 1 - \frac{\exp\left[\left(1 - \frac{\theta(j, t) - \theta_r(j)}{(1-p)[\theta_{fc}(j) - \theta_r(j)]}\right) f_{shape}\right] - 1}{\exp(f_{shape}) - 1} \quad \theta \leq \theta_{fc} \quad (5a)$$

$$k_T(j, t) = 1 \quad \theta > \theta_{fc} \quad (5b)$$

257 where f_{shape} is the shape factor of $k_T(j, t)$ curve, p is the fraction of readily
 258 available soil water relative to the total available soil water. Finally, the salt stress
 259 coefficient $S(j, t)$ for each layer in Eq 3b can be calculated as (Allen et al., 1998; Xue
 260 et al., 2018):

$$S(j, t) = 1 - \frac{B}{100 k_y} (EC_e(j, t) - EC_{threshold}) \quad (6)$$

261 where k_y is the factor that affects the yield, EC_e is the electrical conductivity of the
 262 soil saturation extract (mS cm^{-1}), $EC_{threshold}$ is the calibrated threshold of the
 263 electrical conductivity of the soil saturation extract when the crop yield becomes
 264 affected by salt (mS cm^{-1}), and B is the calibrated crop specific parameter that
 265 describes the decrease rate of crop yield when EC_e increases per unit below the
 266 threshold. The electrical conductivity of the soil saturation extract can be calculated
 267 as (Rhoades et al., 1989):

$$EC_e = 1.33 + 5.88 \times EC_{1:5} \quad (7)$$

268 where $EC_{1:5}$ is the electrical conductivity of the soil extract that soil samples mixed
 269 with distilled water in a proportion of 1:5.

270 2.3.2 VADOSE Module

271 For modeling the daily soil moisture content and groundwater depth, first we need
 272 calculate the soil moisture content at field capacity and the drainable porosity based
 273 on the soil moisture characteristic curve. Besides, considering the water and salt

274 movement is different when there have irrigation and/or precipitation, we simulate the
275 daily soil moisture content and salt with downward flux or upward flux.

276 2.3.2.1 Parameters based on soil moisture characteristic curve for modeling

277 Moisture content at field capacity

278 Field capacity with a shallow groundwater is different than in soils with deep
279 groundwater where water stops moving when the hydraulic conductivity becomes
280 limiting at -33 kPa. When the groundwater is shallow, the hydraulic conductivity is not
281 limiting and the water stops moving when the hydraulic potential is constant and thus
282 the matric potential is equal to the height above the water table (Gardner 1958;
283 Gardner et al., 1970a, b; Steenhuis et al. 1988; Liu et al., 2019). Assuming a unique
284 relationship between moisture content at field capacity and matric potential (i.e. soil
285 characteristic curve), the moisture content at field capacity at any point above the
286 water table is a unique function of the water table depth. Thus, any water added
287 above field capacity will drain downward. When the groundwater is recharged, the
288 water table will rise and increase the moisture contents at field capacity throughout
289 the profile.

290 The moisture contents at field capacity were found by Liu et al. (2019) using the
291 simplified Brooks and Corey soil characteristic curve (Brooks and Corey, 1964)

$$\theta = \theta_s \left[\frac{\varphi_m}{\varphi_b} \right]^{-\lambda} \quad \text{for } |\varphi_m| > |\varphi_b| \quad (8a)$$

$$\theta = \theta_s \quad \text{for } |\varphi_m| \leq |\varphi_b| \quad (8b)$$

292 in which θ is the soil moisture content ($\text{cm}^3 \text{ cm}^{-3}$), θ_s is the saturated moisture

293 content ($\text{cm}^3 \text{cm}^{-3}$), φ_b is the bubbling pressure (cm), φ_m is matric potential (cm),
 294 and λ is the pore size distribution index. The moisture content at field capacity,
 295 $\theta_{fc}(z, h)$, for any point, z , from the surface water for a groundwater at depth, h , can be
 296 expressed as (Liu et al. 2019)

$$\theta_{fc}(z, h) = \theta_s(z) \left[\frac{h-z}{\varphi_b} \right]^{-\lambda} \quad \text{for } |h-z| > |\varphi_b(z)| \quad (9a)$$

$$\theta_{fc}(z, h) = \theta_s(z) \quad \text{for } |h-z| \leq |\varphi_b(z)| \quad (9b)$$

297 where h (cm) is the depth of the groundwater and z (cm) is the depth of the point
 298 below the soil surface. Thus $(h-z)$ is the height above the groundwater and this is
 299 equal to the matric potential for soil moisture content at field capacity.

300 For shallow groundwater, the matric potential at the surface is -33kPa when the
 301 groundwater is 3.3 m depth. For this matric potential, as mentioned above, the
 302 conductivity becomes limiting. This depth of the groundwater is therefore the lower
 303 limit over which the VADOSE module is valid.

304 Evapotranspiration can lower the soil moisture content below field capacity. Thus,
 305 the maximum moisture content in the VADOSE module is determined by the soil
 306 characteristic curve and the height of the groundwater table, and the minimum is the
 307 wilting point that can be obtained by evapotranspiration by the crop. Note that the
 308 saturated hydraulic conductivity does not play a role in determining the moisture
 309 content because inherently it is assumed that it is not limiting in the distribution of the
 310 water.

311 Drainable porosity

312 The drainable porosity is a crucial parameter in modelling the groundwater depth and
 313 soil moisture content. According to the soil water characteristic curve at field capacity,
 314 the drainable porosity can be expressed as a function of the depth. The drainable
 315 porosity is obtained by calculating the field capacity, $W_{fc}(h)$ (cm) for each layer at all
 316 groundwater depths. The total water content at field capacity of the soil profile over a
 317 prescribed depth with a water table at depth h can be expressed as:

$$W_{fc}(h) = \sum_{j=1}^n [L(j) \theta_{fc}(j, h)] \quad (10)$$

318 where $\theta_{fc}(j, h)$ is the average moisture content at field capacity of layer j that can be
 319 found by integrating Eq. 8 from the upper to the lower boundary of the layer and
 320 dividing by the length $L(j)$ which is the height of layer j . The matric potential at the
 321 boundary is equal to the height above the water table. The drainable porosity, $\mu(h)$,
 322 which is a function of the groundwater depth h , can simply be found as the difference
 323 in water content when the water table is lowered over a distance of $2\Delta h$.

$$\mu(h) = \frac{W_{fc}(h + \Delta h) - W_{fc}(h - \Delta h)}{2\Delta h} \quad (11)$$

324 where $\Delta h = 0.5L(j)$ (cm).

325 2.3.2.2 Downward flux (at times of irrigation and/or precipitation) and model output

326 At this situation, the model can simulate the daily soil moisture content of different
 327 layer, the percolation from the upper layer to the next layer, the recharge to the
 328 groundwater, the soil salt concentration of different layer and the salt concentration of
 329 groundwater and the groundwater depth.

330 Water

331 A downward flux occurs when either the precipitation or irrigation is greater than the
 332 actual evapotranspiration. In this case, upward flux will not occur because the actual
 333 evapotranspiration is subtracted from the input at the surface. We consider two cases
 334 when the groundwater is being recharged and when it is not.

335 When the net flux at the surface (irrigation plus rainfall minus actual
 336 evapotranspiration) is greater than that needed to bring the soil up to equilibrium
 337 moisture content, the groundwater will be recharged and the distance of the
 338 groundwater to soil surface decreases and the moisture content will be equal to the
 339 moisture at field capacity. The fluxes from one layer to the next can be calculated
 340 simply by summing the amount of water needed to fill up each layer below to the new
 341 moisture content at field capacity. Hence, the percolation to groundwater, $R_{gw}(t)$, can
 342 be expressed as:

$$R_{gw}(t) = P(t) + I(t) - E_a(t) - T_a(t) - \sum_{j=1}^n \frac{[\theta_{fc}(j, h) - \theta(j, t - \Delta t)]L(j)}{\Delta t} \quad (12)$$

343 where n is the total number of layers, $\theta(j, t)$ is the average soil moisture content in
 344 day t of layer j ($\text{cm}^3 \text{cm}^{-3}$), $E_a(t)$ is the actual evaporation (mm), $T_a(t)$ is the actual
 345 transpiration (mm), $P(t)$ is the precipitation (mm), and $I(t)$ is the irrigation (mm).

346 When the groundwater is not recharged, the rainfall and the irrigation are added
 347 to uppermost soil layer and when the soil moisture content will be brought up to the
 348 field capacity and the excess water will infiltrate to next soil layer bringing it up to field
 349 capacity. This process continues until all the rainwater is distributed. Formally the soil
 350 moisture can be expressed as

351
$$\theta(j, t) = \min \left[\theta_{fc}(j, h), \left[\theta(j, t - \Delta t) + \frac{R_w(j-1, t) \Delta t}{L(j)} \right] \right] \quad (13)$$

352 where $\theta(j, t)$ is the average soil moisture content in day t of layer j ($\text{cm}^3 \text{cm}^{-3}$),

353 $R_w(j - 1, t)$ is the percolation rate to layer j (mm) and can be found with Eq 12 by

354 replacing $j-1$ for n in the summation sign.

$$R_w(j - 1, t) = P(t) + I(t) - E_a(t) - T_a(t) - \sum_1^{j-1} \frac{[\theta_{fc}(j, h) - \theta(j, t - \Delta t)]L(j)}{\Delta t} \quad (14)$$

355 For the uppermost soil layer, the water percolation can be expressed as

356
$$R_w(0, t) = I(t) + P(t) - E_a(t) - T_a(t) \quad (15)$$

357 Salinity

358 The salt concentration for layer j can be expressed by a simple mass balance as:

$$C(j, t) = \frac{\theta(j, t - \Delta t) C(j, t - \Delta t)L(j) + [R_w(j - 1, t) C(j - 1, t) - R_w(j, t) C(j, t)] \Delta t}{\theta(j, t)L(j)} \quad (16)$$

359 where $C(j, t)$ is the salt concentration of layer j at time t (g L^{-1}). The equation can be

360 rewritten as an explicit function of $C(j, t)$

$$C(j, t) = \left[\frac{\theta(j, t)L(j)}{1 + R_w(j, t) \Delta t} \right] \left[\frac{\theta(j, t - \Delta t) C(j, t - \Delta t)L(j) + R_w(j - 1, t) C(j - 1, t) \Delta t}{\theta(j, t)L(j)} \right] \quad (17)$$

361 For the surface layer $j=1$, we obtain

$$C(1, t) = \left[\frac{\theta(1, t)L(1)}{1 + R_w(1, t)\Delta t} \right] \left[\frac{\theta(1, t)L(1)}{1 + R_w(1, t)\Delta t} \frac{\theta(j, t - \Delta t) C(j, t - \Delta t)L(j) + I(t) C_i \Delta t}{\theta(j, t)L(j)} \right] \quad (18)$$

362 where C_i is the salt concentration in the irrigation water (g L^{-1}).

363 The salt concentration of the groundwater $C_{gw}(t)$ can be estimated as:

$$C_{gw}(t) = \frac{[G(t - 1) \times C_{gw}(t - 1) + C(5, t) \times R_w(t)]}{G(t - 1) + R_w(t)} \quad (19)$$

364 Where $C(5, t)$ is the soil salinity concentration of the soil layer 5 on day t (g L^{-1}),

365 $G(t - 1)$ is the difference of the groundwater depth and the depth that the largest

366 groundwater table fluctuations depth of groundwater table on day $(t-1)$ (m) (Xue et al.,

367 2018), $C_{gw}(t)$ is the soluble salt concentration of groundwater at day t (g L^{-1}).

368 2.3.2.3 Upward flux and model output

369 For the upward flux period, the downward water flux to groundwater is zero. The
370 evapotranspiration leads to the decrease of soil moisture content in the vadose zone
371 and lowers the groundwater table due to the upward movement of groundwater to
372 crop root zone and soil surface. The soil moisture content is calculated by taking the
373 difference of equilibrium moisture content associated with the change of groundwater
374 depth. At this situation, the model can output the daily soil moisture content of
375 different layer, the upward groundwater flux, the groundwater depth, the soil salt
376 concentration of different layer and the salt concentration of groundwater.

377 Water

378 The groundwater upward flux, $U_{gw}(h, t)$, is limited by either the maximum upward
379 flux of groundwater, $U_{gw,max}(h)$, or the actual evapotranspiration, formally stated as:

$$U_{gw}(h, t) = \min [[E_a(t) + T_a(t)], U_{gw,max}(h)] \quad (20)$$

$$E_a(t) = \sum_{j=1}^n E_a(j, t) \quad (21)$$

$$T_a(t) = \sum_{j=1}^n T_a(j, t) \quad (22)$$

380 where $U_{gw,max}(h)$ is the actual upward flux from groundwater (mm), $E_a(t)$ is the
381 actual evaporation at day t (mm), $T_a(t)$ is the actual transpiration at day t (mm),
382 $E_a(j, t)$ is the actual evaporation at day t of layer j (mm) and $T_a(j, t)$ is the actual
383 transpiration at day t of layer j (mm).

384 The maximum upward flux can be expressed as (Liu et al., 2019; Gardner et al.,

385 1958)

$$U_{gw,max}(h) = \frac{a}{e^{bh} - 1} \quad (23)$$

386 where a and b are constants that need to be calibrated, h is the groundwater depth
387 (cm).

388 Two cases are considered for determining the moisture contents of the layers
389 depending on whether the actual evapotranspiration is greater or less than the
390 maximum upward flux.

391 Case I: $U_{gw,max}(h) > E_a(t) + T_a(t)$

392 In this case, where the maximum upward flux is greater than the evaporative demand,
393 the groundwater depth is updated

$$h(t) = h(t - \Delta t) + \frac{E_a(t) + T_a(t)}{\mu(\bar{h})} \quad (24)$$

394 where $\mu(\bar{h})$ is the average drainable porosity over the change in groundwater depth
395 h . The moisture content after the change in groundwater depth becomes

$$\theta(j, t) = \theta(j, t - \Delta t) + \theta_{fc}(j, h(t)) - \theta_{fc}(j, h(t - \Delta t)) \quad (25)$$

396 Note that when the layer is at field capacity and the upward flux is equal to the
397 evaporative flux, the layer remains at field capacity for the updated groundwater
398 depth at time t .

399 Case II: $U_{gw,max}(h) \leq E_a(t) + T_a(t)$

400 In this case, the groundwater depth is updated

$$h(t) = h(t - \Delta t) + \frac{U_{gw,max}(h)}{\mu(\bar{h})} \quad (26)$$

401 When the upward flux is less than the sum of the actual evaporation and transpiration,

402 the moisture content is updated with the difference between the two fluxes,
 403 $U_{gw,max}(h)$ and $[E_a(t) + T_a(t)]$, according to a predetermined distribution extraction of
 404 water out of the root zone

$$\theta(j, t) = \theta(j, t - \Delta t) + \theta_{fc}(j, h(t)) - \theta_{fc}(j, h(t - \Delta t)) - \frac{r(j)[E_a(t) + T_a(t) - U_{gw,max}(h)]}{L(j)} \quad (27)$$

405 The upward flux of water can be found by summing the differences in moisture
 406 content above the layer j similar to Eq 14, but starting the summation at the
 407 groundwater.

408 Salinity

409 The salt from groundwater is added to the soil layers according to the root function.

410 The soil salinity concentration in layer j at day t can be expressed as

$$C(j, t) = \frac{\theta(j, t - \Delta t) C(j, t - \Delta t) L(j) + r(j, t) U_g(h, t) C_{gw}(t)}{\theta(j, t - \Delta t) L(j) + (\theta_{fc}(j, h(t)) - \theta_{fc}(j, h(t - \Delta t))) L(j) - r(j, t) (E_a(t) + T_a(t) - U_{gw,max}(h))} \quad (28)$$

411 Since water is extracted from the reservoir that has the same concentration as in the
 412 reservoir, the concentration will not change, hence the equation used to estimate the
 413 groundwater salt concentration can be expressed as

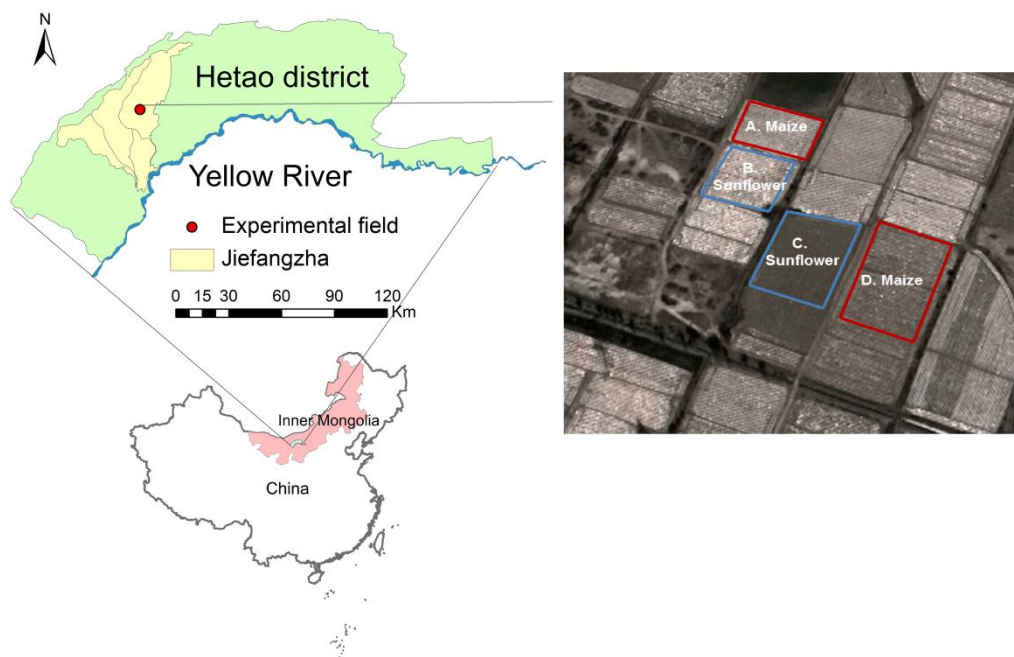
$$414 \quad C_{gw}(t) = C_{gw}(t - \Delta t) \quad (29)$$

415 3. Data collection

416 3.1 Study area

417 Field experiments were conducted in 2017 and 2018 in Shahaoqu experimental
 418 station in Jiefangzha sub-district, Heato irrigation district in Inner Mongolia, China (Fig.
 419 3). Irrigation water originates from the Yellow River. The area has an arid continental
 420 climate. Mean annual precipitation is 155 mm a⁻¹ of which 70% falls from June to
 421 September. Pan evaporation is 2000 mm a⁻¹ (Xu et al., 2010). The mean annual

422 temperature is 7°C. The soils begin to freeze in the middle of November and to thaw in
423 end of April or beginning of May. Maize, wheat and sunflower are the main crops in
424 Jiefangzha sub-district and are grown with flood irrigation. The groundwater depth is
425 between 0.5-3 m. Regional exchange of groundwater is minimal due to low gradient
426 of 0.01-0.025 (Xu et al., 2010). Thus, the groundwater flows mainly vertically with
427 minimum lateral flow in the regional scale. Over 50% of the total irrigated cropland,
428 5250 km² in the Hetao irrigation district in the Yellow River basin, is affected by
429 salinity (Feng et al., 2005).



430
431 Fig. 3 Location of the Shahaoqu experimental field (Note: The figure was downloaded
432 from Google earth. The imagery is taken on April 8, 2019)

433 3.2 Field observations and data

434 The layout of the experimental fields is shown in Figure 3. The areas of fields A, B, C
435 and D are 920, 2213, 1167, 1906 m², respectively. Field A and D were planted with
436 maize on May 10 and harvested on September 30, 2017. In 2018, fields A and D were

437 planted with gourds and were therefore not monitored in 2018. Fields B and C were
 438 seeded with sunflower in both 2017 and 2018. The sunflower was planted on June 1,
 439 2017 and June 5, 2018. Harvest was on September 15 in both years. The fields were
 440 irrigated by flooding the field ranging from two to five times during the growing season
 441 (Table 1). A well was installed in each experimental field to monitor the groundwater
 442 depth.

443 Table 1 Irrigation scheduling for the Shahaoqu experimental fields in 2017 and 2018

Field	Year	Irrigation events	Date	Irrigation depth (mm)
A (maize)	2017	1	5/30	100
		2	6/25	162
		3	7/14	275
		4	8/6	199
	2017	1	6/26	140
		2	7/23	121
B (sunflower)	2018	1	6/20	134
		2	6/24	60
		3	7/15	114
		4	7/22	40
		5	8/31	130
C (sunflower)	2017	1	6/19	80
		2	6/30	80
	2018	1	6/20	140
		2	7/14	100
D (maize)	2017	1	6/13	150
		2	6/26	94
		3	7/6	50
		4	7/14	174
		5	8/6	120

444

445 Daily meteorological data, including air temperature, precipitation, relative
 446 humidity, wind speed, and sunshine duration, originated from the weather station at
 447 the Shahaoqu experimental station. The soil moisture content for the four

448 experimental fields in 2017 and for field C in 2018 during the crop growing season
449 was measured every 7-10 days at the depths of 0-20, 20-40, 40-60, 60-80, 80-100 cm
450 by taking soil samples and oven drying. In 2018, in addition, the soil moisture content
451 at same depths was monitored daily using Hydra Probe Soil Sensors (Stevens Water
452 Monitoring System Inc., Portland, OR, USA) in field B except the oven drying method.
453 The Hydra Probe was calibrated using the intermittent manual measurements. In
454 2017, the groundwater depths were manually measured in all four experimental fields
455 about every 7-10 days. In 2018, the groundwater depth in fields B and C was
456 recorded at 30 min intervals using an HOBO Water Level Logger-U20 (Onset, Cape
457 Cod, MA, USA). The sensors of the soil moisture content and groundwater depth
458 were connected to data loggers and downloaded via wireless transmission. The crop
459 leaf area and crop height were manually measured every 7-12 days.

460 Undisturbed soil samples were collected in 5 cm high rings with a diameter of 5.5
461 cm from the five soil layers where the soil moisture were taken and used for textual
462 analysis, saturated soil moisture content, field capacity and soil bulk density. The soil
463 texture was analyzed with a laser particle size analyzer (Mastersizer 2000, Malvern
464 Instruments Ltd., United Kingdom). The American soil texture classification method
465 was used in this study. Finally, the soil samples were collected 7-10 days apart to
466 monitor the change of electrical conductivity (EC). The soil samples were mixed with
467 distilled water in a proportion of 1:5 to measure the electrical conductivity of the soil
468 water by a portable conductivity meter. It is assumed that 1 ms cm^{-1} corresponds to
469 640 mg L^{-1} of total dissolved salts (Wallender and Tanji, 2011; Xue et al., 2018).

470 3.3 Model calibration and validation

471 The observed soil moisture contents, groundwater depths, crop heights, LAIs and
472 salinity concentrations for field A with maize and sunflower fields B and C in 2017
473 were used for calibration and the sunflower data of fields B and C in 2018 and the
474 maize data in field D in 2017 were used for validation. The initial θ_{fc} was based on the
475 measured data (Table 2). The initial values of θ_s and θ_r were derived from the soil
476 texture with the method of Ren et al. (2016) (Table2). The default values of EPIC for
477 sunflower and maize were used as initial values for simulating crop growth (K_{cmax} and
478 LAI_{mx} in Eq. S3, K_b in Eq. S4, H_{mx} in Eq. S7, PHU in Eq. S9, T_b in Eq. S10, ad in Eq.
479 S12, T_0 and T_b in Eq. 16, RD_{mx} in Eq. S18). The initial value maximum crop coefficient
480 (K_{cmax}) in Eq. S3 in Supplementary S1 for evapotranspiration calculation was taken
481 from *Sau et al.*, (2004). The initial values of two groundwater parameters (a and b in
482 Eq. 23) were based on Liu et al., (2019). The Brooks and Corey soil moisture
483 characteristic parameters (φ_b , λ in Eq. 8) were obtained by fitting the outer envelope
484 of the measure moisture content and water table data.

485 Statistical indicators were used to evaluate goodness of fit of the hydrological
486 model for both calibration and validation (Ritter and Muñoz-Carpena, 2013). The
487 statistical indicators included the root mean square error (RMSE) (Abraham and See,
488 2000),

$$RMSE = \sqrt{\frac{1}{N} \sum_{i=1}^N (P_i - O_i)^2} \quad (30)$$

489 the mean relative error (MRE) (Dawson et al., 2006; Nash and Suscliff, 1970),

$$\text{MRE} = \frac{1}{N} \sum_{i=1}^N \frac{(P_i - O_i)}{O_i} \times 100\% \quad (31)$$

490 the Nash-Sutcliffe efficiency coefficient (NSE) (Nash and Suscliff, 1970),

$$\text{NSE} = 1 - \frac{\sum_{i=1}^N (P_i - O_i)^2}{\sum_{i=1}^N (O_i - \bar{O})^2} \quad (32)$$

491 and the determination coefficient (R^2) and regression coefficient (b) (Xu et al., 2015)

$$R^2 = \left[\frac{\sum_{i=1}^N (O_i - \bar{O})(P_i - \bar{P})}{[\sum_{i=1}^N (O_i - \bar{O})]^{0.5} [\sum_{i=1}^N (P_i - \bar{P})]^{0.5}} \right]^2 \quad (33)$$

$$b = \frac{\sum_{i=1}^N O_i \times P_i}{\sum_{i=1}^N O_i^2} \quad (34)$$

492 where N is the total number of observations; P_i and O_i are the i^{th} model predicted and
 493 observed values ($i=1,2,3\dots N$), respectively; \bar{O} and \bar{P} are the mean observed values
 494 and predicted values, respectively. The RMSE is used to evaluate the bias of the
 495 measured data and predicted data. The MRE can evaluate the credibility of the
 496 measured data. The NSE is usually used to evaluate the quality of the hydrological
 497 models. The R^2 is used to measure the fraction of the dependent variable total
 498 variation that can be explained by the independent variable. And the regression
 499 coefficient represents the influence of the independent variable on the dependent
 500 variable in the regression equation. The value of RMSE and MRE close to 0 indicates
 501 good model performance. The value of NSE ranges from $-\infty$ to 1. NSE=1 means a
 502 perfect fit while the negative NSE value indicates the mean observed value is a better
 503 predictor than the simulated value (Moriasi et al., 2007). For b and R^2 , the value
 504 closest to 1 indicates good model predictions.

505 3.4 Parameters sensitivity analysis

506 A sensitivity analysis was performed to determine how the input parameters
507 affected output of the models (Cloke et al., 2008; Cuo et al., 2011). Each parameter
508 was varied over a range of -30% to 30% to derive the corresponding impact on the
509 model output of soil moisture, groundwater depth, soil salinity, leaf area index and
510 actual evapotranspiration. The change in output values was plotted against the
511 change in input values.

512 **4 Results**

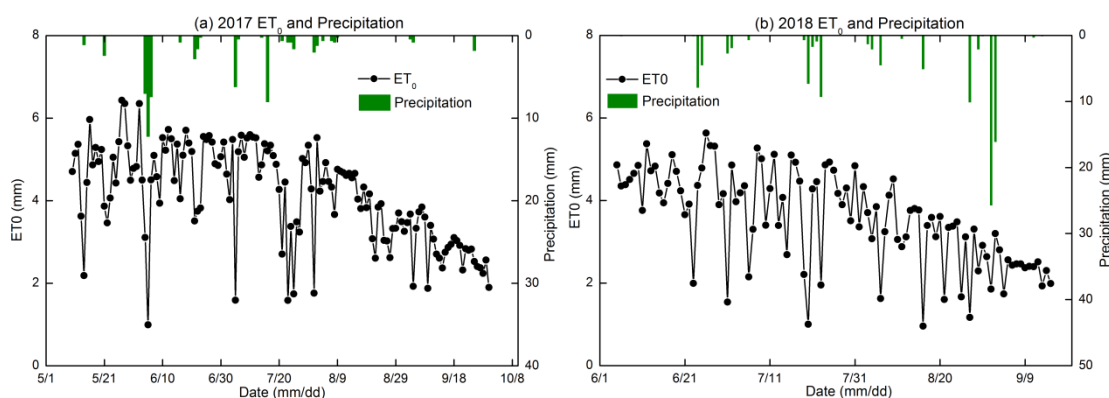
513 The 2017 and 2018 experimental data of the Shahaqu farmers' fields in the
514 Hetao irrigation district (Fig.3) are presented first, followed by the calibration and
515 validation results of the CROP and VADOSE modules of EPICS model.

516 4.1 Results of the field experiment

517 4.1.1 Water input

518 The precipitation was 63 mm in 2017 (May 10 to September 30) and 108 mm in
519 2018 (June 1 to September 15). The precipitation from the greatest rainstorm was 26
520 mm on September 1, 2018 (Fig. 4). Irrigation provided most of the water for the crops.
521 Field A (maize) was irrigated four times with a total of 736 mm and field D (maize) was
522 irrigated five times for a total of 588 mm in 2017. Sunflower fields B and C were both
523 irrigated twice with a total water amount of 261mm and 160mm, respectively, in 2017.
524 In 2018, fields B and C were irrigated five and two times, respectively, with a total
525 water amount of 478mm and 240mm, respectively. The reference evapotranspiration
526 ranged from 1 mm d⁻¹ to a maximum of 6.4 mm d⁻¹ during crop growing period (Fig. 4).
527 The total reference evapotranspiration from May 10 to September 30, 2017 was 595

528 mm and 368 mm from June 1 to September 15, 2018. The reason was that there
 529 were more rainfall days in June, July and September in 2018 than in 2017, which
 530 increased the amount of water available for the evapotranspiration by the crop in
 531 2018. In addition, the wind speed was high in May that increase the
 532 evapotranspiration was elevated. In the study of Ren et al. (2017) and Miao (et al.
 533 2016), the mean ET_0 was over 6 mm per day on May. Hence, the ET_0 during the study
 534 period in 2017 was greater than in 2018.



535
 536 Fig 4. Reference evapotranspiration (ET_0) and precipitation during crop growth period
 537 in 2017 and 2018.

538
 539 4.1.2 Soil physical properties

540 Based on the soil textural analysis in Table 2, the soils were classified as silt, silt loam
 541 and loamy sand. Bulk densities varied from 1.24 to 1.47 $Mg\ m^{-3}$ with the greatest bulk
 542 densities in the 0-20 cm soil layer. There was generally more sand in the top 40 cm
 543 than below. The subsoil was heavier and had the greatest percentage of silt (Table 2).
 544 The moisture content at -33 kPa (0.33 bar) varied from 0.25 to 0.35 $cm^3\ cm^{-3}$ and at
 545 1.5Mpa (wilting point at 15 bar) ranged from 0.08 to 0.15 $cm^3\ cm^{-3}$ (Table 2).

546 Table 2 Soil texture and bulk density of the experimental fields in Shahaoqu

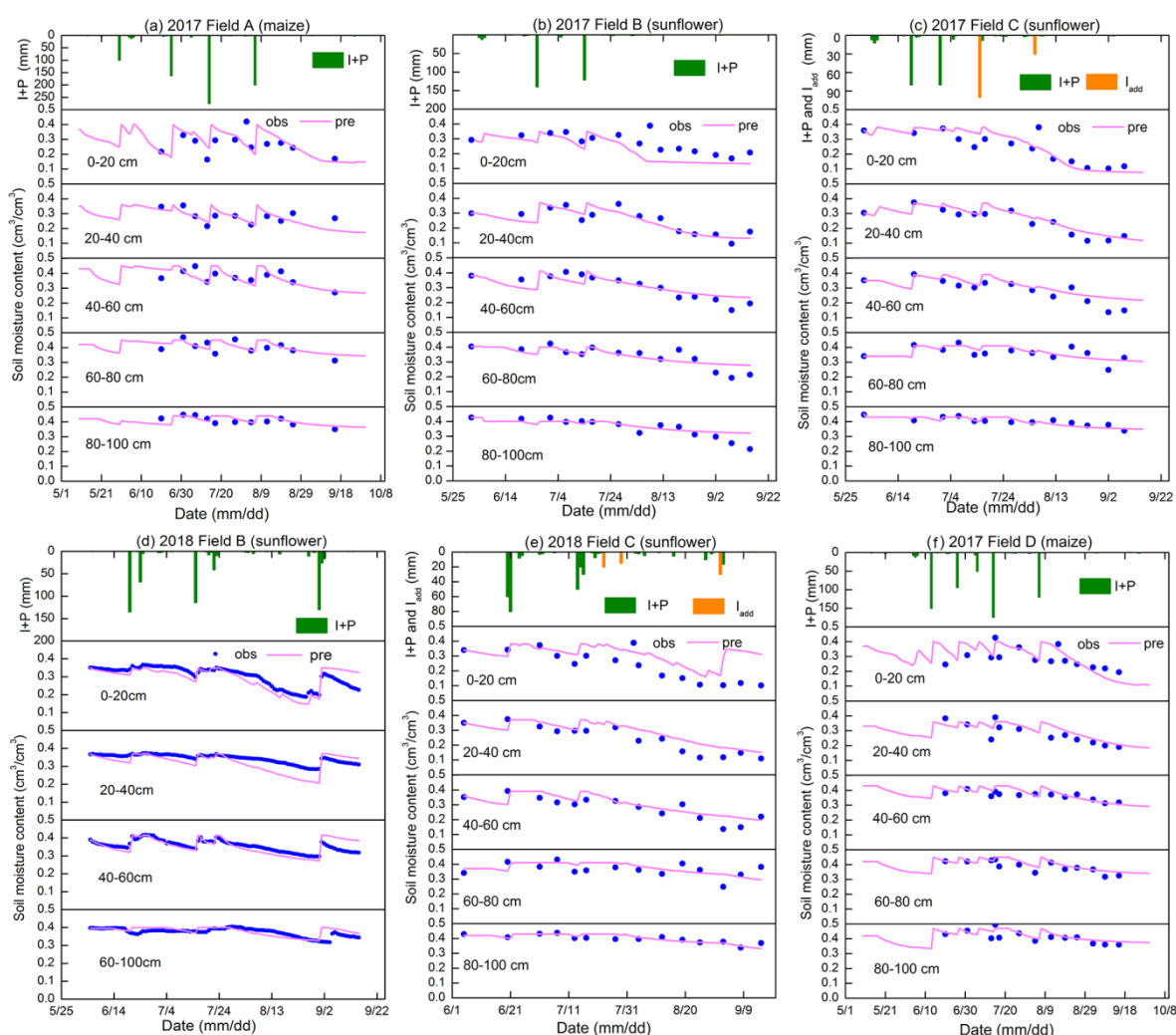
Field	Soil depth (cm)	Sand(%)	Silt(%)	Clay(%)	Soil type	ρ (Mg m ⁻³)	θ_{fc} (m ³ m ⁻³)	θ_r (m ³ m ⁻³)
A	0-20cm	26	62	13	Silt loam	1.44	0.31	0.1
	20-40cm	76	22	2	Loamy sand	1.24	0.32	0.07
	40-60cm	10	79	10	Silt loam	1.33	0.33	0.12
	60-100cm						0.34	0.14
			6	79	15	Silt loam	1.35	0.35
B	0-20cm	22	64	13	Silt loam	1.44	0.29	0.15
	20-40cm	16	73	11	Silt loam	1.24	0.26	0.13
	40-60cm	18	73	9	Silt loam	1.33	0.32	0.11
	60-80cm	8	77	16	Silt	1.35	0.34	0.14
	80-100cm	13	79	8	Silt loam		0.35	0.12
C	0-20cm	29	63	8	Silt loam	1.47	0.26	0.08
	20-40cm	37	56	6	Silt loam	1.33	0.25	0.08
	40-60cm	35	59	7	Silt loam	1.32	0.26	0.08
	60-80cm	14	74	12	Silt loam	1.38	0.31	0.12
	80-100cm	10	82	8	Silt	1.38	0.34	0.11
D	0-20cm	27	62	11	Silt loam	1.47	0.3	0.15
	20-40cm	5	80	15	Silt loam	1.33	0.27	0.14
	40-60cm	7	75	18	Silt loam	1.32	0.33	0.15
	60-100cm						0.34	0.12
		10	81	9	Silt	1.38	0.31	0.14

547

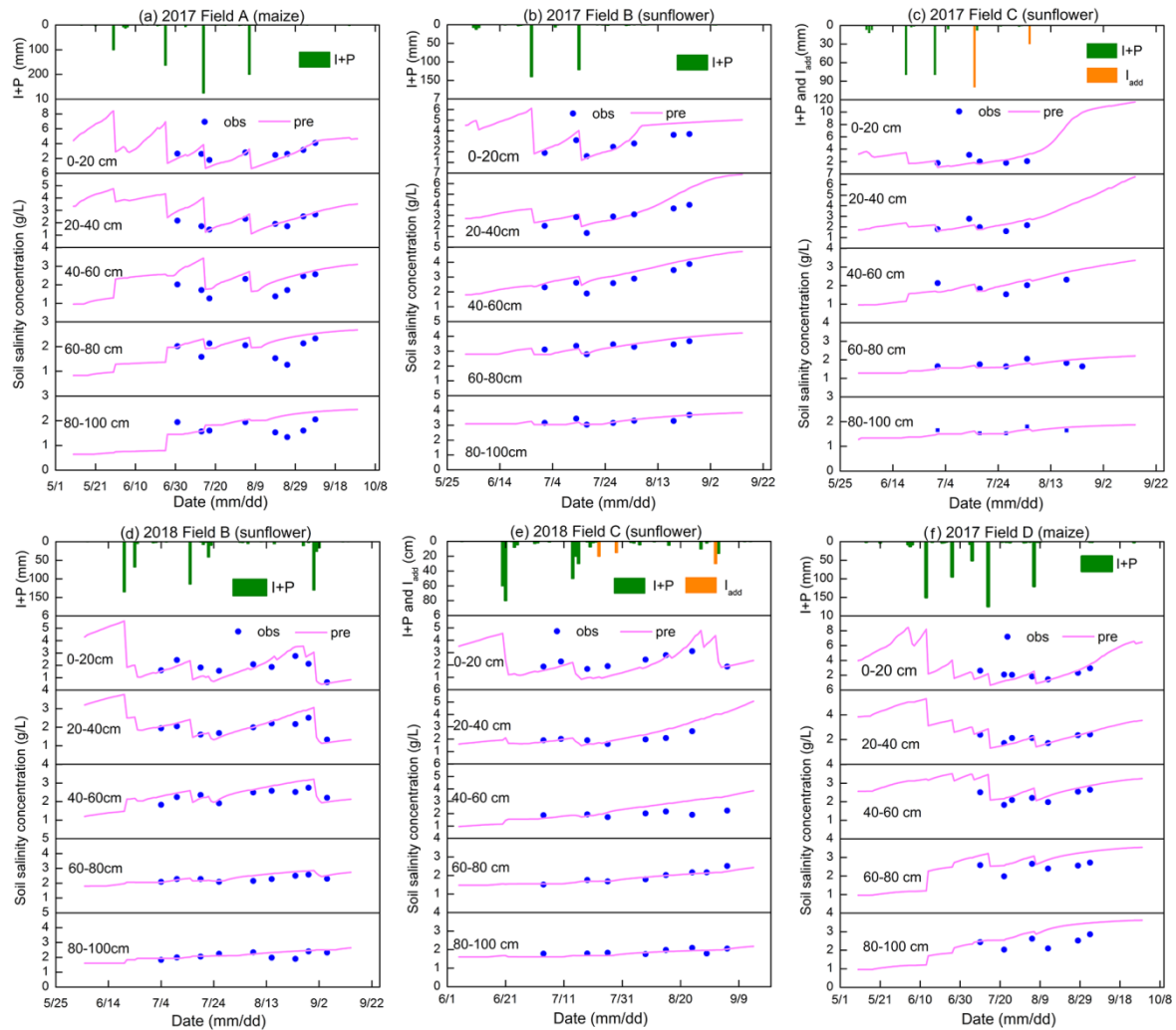
548 4.1.3 Soil moisture content

549 Moisture content, rainfall and irrigation amounts are depicted for the five layers
550 and the four fields in 2017 and two fields in 2018 in Fig. 5. Blue closed spheres
551 indicate that the moisture content was determined on cored soil samples (Figs. 5a, b,
552 c, e, f) and close-spaced spheres when the hydra probe was used (Fig. 5d). The
553 moisture contents were near saturation when irrigation water was added and
554 subsequently decreased due to crop transpiration and soil evaporation (Fig. 5). In all
555 cases, the moisture contents during the main growing period remained above the
556 moisture content at -33 kPa that ranged from 0.25 cm³cm⁻³ to 0.34 cm³cm⁻³ for the

557 60-80 cm depth (Table 2, Fig.5). Only after the last irrigation and during harvest of the
 558 crop did the moisture content in the top 0-40 cm for maize and 0-60 cm for sunflower
 559 decrease below the moisture content at -33kPa. During the growing season, the
 560 variation of moisture content was greater in the top 60 cm with the majority of the
 561 roots than in the lower depths where, after the first irrigation, it remained nearly
 562 constant close to saturation.



563
 564 Fig. 5 Observed (blue dots) and simulated soil moisture content of the Shahaoqu
 565 experimental fields during model calibration (a,b,c) and validation (d,e,f)



566

567 Fig. 6 Observed (blue dots) and simulated soil salinity concentration of the
 568 experimental fields in Shahaoqu during model calibration (a,b,c) and validation (d,e,f).

569 4.1.4 Salinity

570 Overall the salt concentration is greatest at the surface and increases at all
 571 depths during the growing season. Sunflower is more salt tolerant than maize and the
 572 overall salt concentration was greater in the sunflower fields (Fig. 6) at comparable
 573 times of the crop development for field B but not for field C. Comparing the salt
 574 concentration and soil moisture patterns (Fig.5), we note that they behave similarly
 575 but opposite to each other (Fig. 6). The soil salinity concentration was decreasing

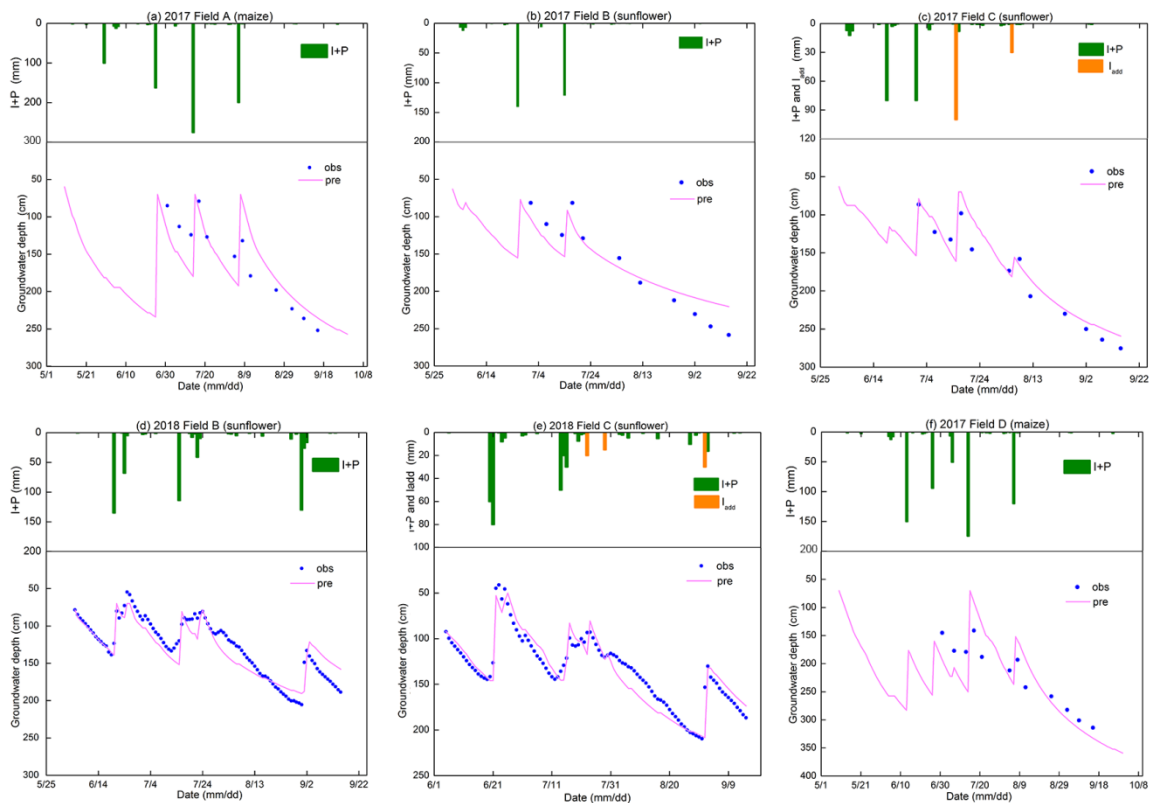
576 during an irrigation event due to dilution and then gradually increasing partly due to
577 evaporation of the water. Some of the soil salt was transported to the layers below
578 during irrigation and some salt was moving upward with the evaporation from the
579 surface. As expected, after the harvest, the autumn irrigation decreased the salt
580 concentration from fall 2017 to spring 2018.

581 4.1.5 Groundwater observations

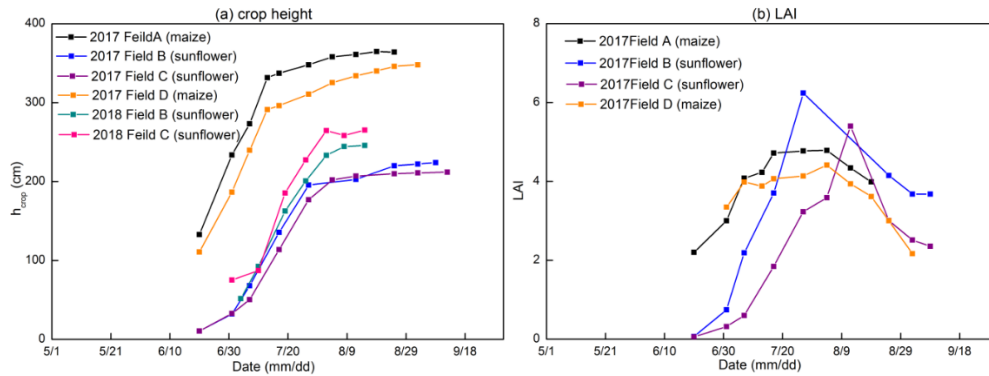
582 The variation in groundwater depth during the growing season was very similar
583 for both years and in all fields. The groundwater depth for all fields was between 50
584 and 100 cm from the surface after an irrigation event and then decreased to around
585 150 cm before the next irrigation or rainfall (Fig.7). Only after the last irrigation in
586 August 2017 did the water table decrease to below 250 cm and to around 200 cm in
587 2018. Field D followed the same pattern but the groundwater was more down from
588 the surface. In several instances, the groundwater table increased without an
589 irrigation or rainfall event in sunflower field C (Fig. 7c and 7e). This was likely related
590 to an irrigation event either from [an irrigation in nearby field that affected the overall](#)
591 [water table](#) or an accidental irrigation that was not properly documented. We
592 estimated the amount of irrigation water based on the change in moisture content in
593 the soil profile (orange bars in Fig. 7c and 7e). Finally, there was a notable rise in the
594 water table of an mean 375mm “autumn irrigation” after harvest between the end of
595 2017 (Figs. 7 a, b, c) and the beginning of 2018 (Figs. 7 d, e, f), which is a common
596 practice in the Jiefangzha irrigation district to leach the salt that has accumulated in
597 the profile during the growing periods.

598 Note that in Fig. 7, after an irrigation event, the groundwater depth was between
 599 50-80 cm while the whole profile was saturated (Fig. 5). This is directly related to the
 600 bubbling pressure of the water. After the irrigation event stopped, the water table was
 601 likely at the surface but then immediately decreased because a small amount of
 602 evaporated water will bring the water table down to a depth of approximately equal to
 603 the bubbling pressure, φ_b , in Eq. 5. The bubbling pressures are listed in Table 3.
 604 4.1.6 LAI and plant height

605 Plant height and LAI followed the typical growth curve that started slowly to rise
 606 in the beginning, accelerated during the vegetative stage and then became constant
 607 during the seed setting and ripening stages (Fig. 8). In the maturing stage, the leaf
 608 area index decreased.



609
 610 Fig. 7. Observed (blue dots) and simulated groundwater depth of the experimental
 611 fields in Shahaqu during model calibration (a, b, c) and validation (d, e, f)



612

613 Fig. 8 Observed crop height (a) and leaf area index (b) of the experimental field in
 614 Shahaoqu in 2017 and 2018.

615

616 4.2 Soil Characteristic curve and drainable porosity

617 To simulate the soil moisture content and to derive drainable porosity as a function of
 618 water table depth, the soil moisture characteristic curves were derived by plotting the
 619 observed soil moisture content in 2017 and 2018 versus the height above the water
 620 table to the soil surface for the five soil layers in Fig. 9. The Brooks-Corey equation
 621 (Brooks and Corey, 1964) was fitted through outer envelope of the points. The
 622 parameters of the Brooks-Corey equation were adjusted through a trial and error to
 623 obtain the best fit (Table 3a). In Fig. 9, points on the left side of the soil moisture
 624 characteristic curve (moisture content smaller than the field capacity) were due to
 625 water removal at times when evaporative demand was greater than the upward water
 626 flux. Under these conditions the conductivity is limiting in the soil and there is no
 627 relationship between groundwater depth and matric potential. Since we take the
 628 water table depth as proxy for matric potential, these points are omitted when drawing
 629 the soil characteristic curve. The few points at the right of the soil moisture
 630 characteristic curve indicate the soil moisture was greater than field capacity and

631 matric potential and groundwater were not yet at equilibrium after an irrigation event.

632 The fitted parameter values are consistent. Field A had a greater bubbling
 633 pressure and moisture content at -33 kPa than the other fields indicating that this field
 634 had more clay. This was confirmed by the data in Table 2. For fields B, C and D, the
 635 bubbling pressure was greater at the 60-80 cm depth or the 80 -100 cm depth, which
 636 was also in accordance with the data in Table 2.

637 Table 3a Calibrated soil hydraulic parameters in the Brooks and Corey soil moisture
 638 characteristic curve.

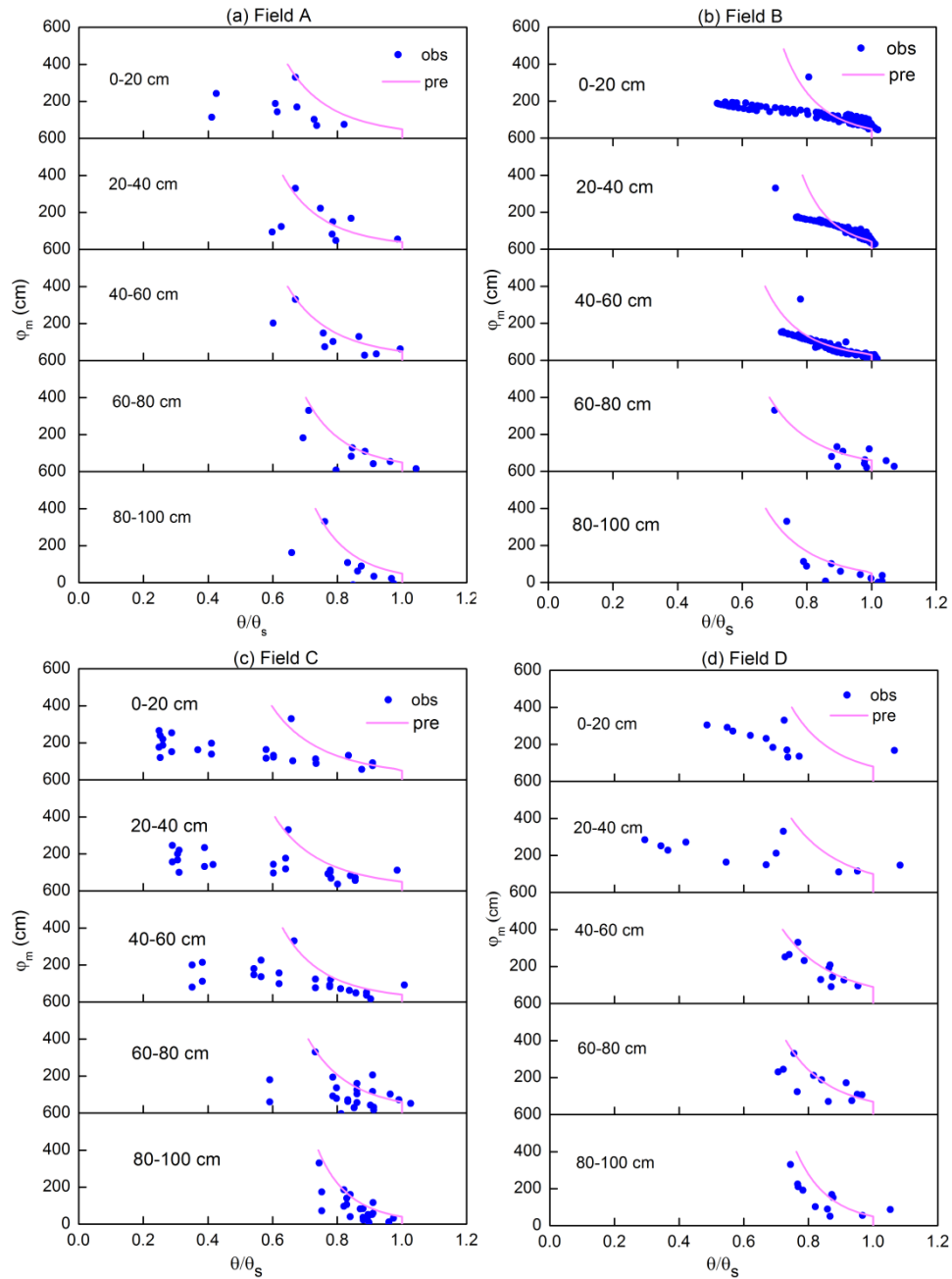
Field	Parameter	0-20cm	20-40cm	40-60cm	60-80cm	80-100cm
A	θ_s	0.4	0.36	0.43	0.45	0.47
	φ_b	80	100	90	70	50
	λ	0.18	0.21	0.22	0.18	0.15
B	θ_s	0.35	0.37	0.41	0.4	0.4
	φ_b	50	55	33	60	55
	λ	0.14	0.11	0.16	0.2	0.2
C	θ_s	0.38	0.37	0.39	0.71	0.43
	φ_b	55	50	40	60	40
	λ	0.26	0.24	0.2	0.18	0.13
D	θ_s	0.4	0.36	0.45	0.45	0.44
	φ_b	50	40	55	50	50
	λ	0.21	0.2	0.3	0.17	0.15

639 Note: θ_s is the soil moisture at saturation ($\text{cm}^3\text{cm}^{-3}$), φ_b is bubbling pressure (cm), λ is
 640 the pore size distribution index.

641 Table 3b Calibrated groundwater parameters

Field\parameters	A	B	C	D
a	70	75	110	70
b	0.02	0.025	0.022	0.015

642



643

644 Figure. 9 Soil moisture characteristic curves of five soil layers in the experimental
 645 fields. The pink line is the fit with the Brooks-Corey equation.

646

647 4.3 Parameters sensitivity analysis

648 The results of sensitivity analysis of the 15 input parameters on 5 output parameters

649 are shown in Fig. 10. The evaluated output parameters are soil moisture content,

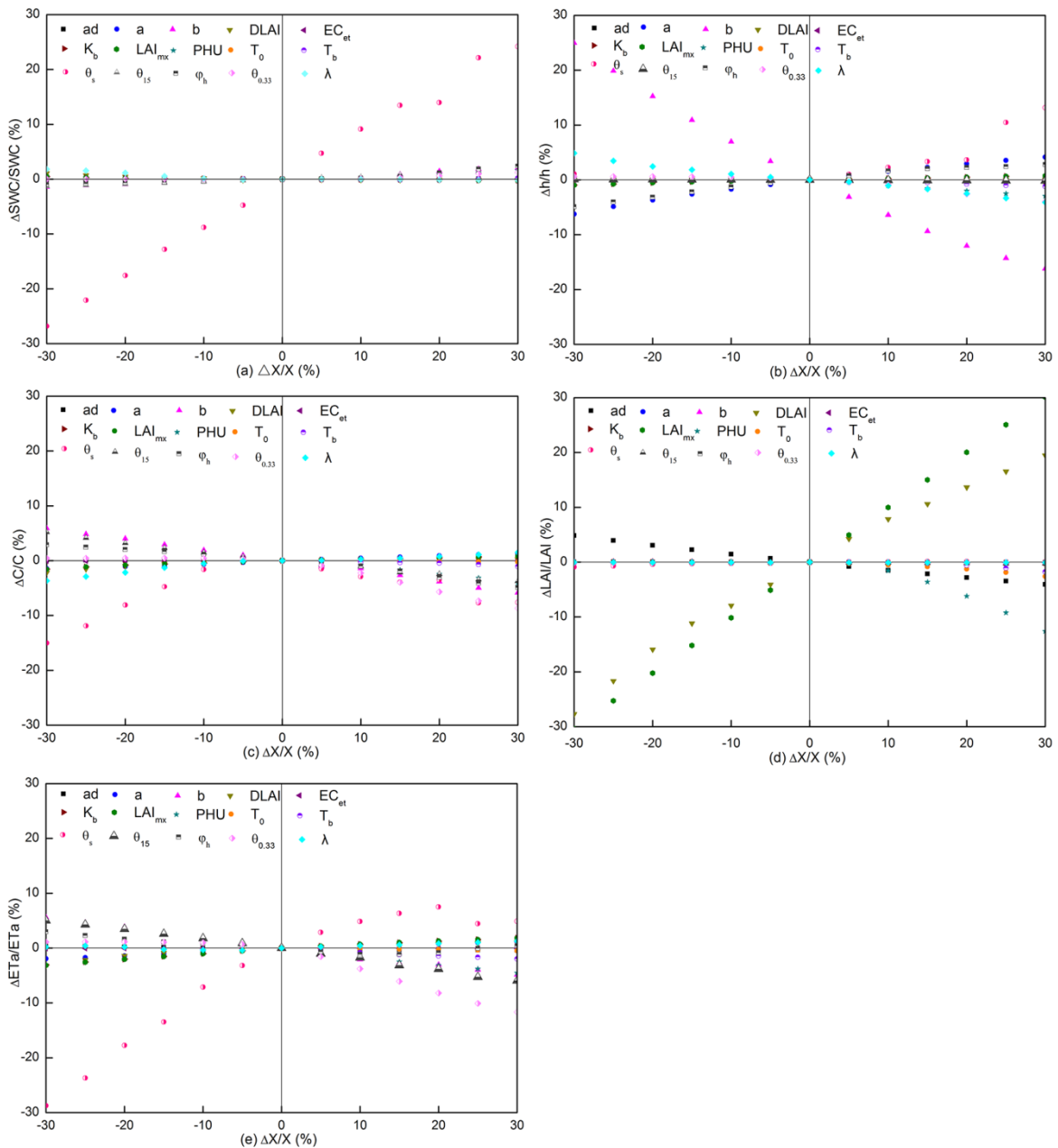
650 groundwater depth, soil salinity concentration, field evapotranspiration, and crop leaf

651 area index (LAI). Steeper lines indicate a greater sensitivity of the parameter.

652 The results of the sensitivity analysis show that moisture content predictions (Fig
653 10a) are the most sensitive to the input value of the saturated moisture content (θ_s).
654 None of the other parameters are very sensitive. This includes the shape parameters
655 for the soil characteristic curve, bubbling pressure φ_b , and the exponent λ . The input
656 parameter with the most sensitivity for *groundwater depth* (Fig. 10b), is the saturated
657 moisture content as well. Other less sensitive parameters are the exponent b and
658 constant a in Eq. 23 in predicting the upward flux and the bubbling pressure, φ_b , of the
659 soil moisture characteristic curve (Eq. 8a). Likewise, in case of the *salinity* predictions
660 (Fig. 10c), the saturated moisture content gives the greatest relative change in salt
661 content. Less sensitive, but still important, are the field capacity, θ_{fc} , the bubbling
662 pressure, φ_b , and the exponent λ of the soil characteristic curve (Eq. 8a) and b in Eq.
663 23. The sensitive parameters for the *leaf area index (LAI)* (Fig 10d) are the maximum
664 potential leaf area index, LAI_{mx} , and fraction of growing season when leaf area
665 declines (*DLAI*) followed by total potential heat units required for crop maturation
666 (*PHU*). Finally, for the *evapotranspiration* (Fig 10e), the saturated soil moisture
667 content is the most sensitive parameter, and other less sensitive parameters are the
668 exponent b and field capacity.

669 Thus, the model output is most sensitive to the input parameters that define the
670 soil hydraulic properties, groundwater flux and crop growth. As expected, since the
671 soil remains near field capacity, the parameters that relate to the reduction of
672 evaporation when the soil dries out are insensitive. When used in the simulation

673 practices, the model needs to be calibrated and verified to avoid high error from
 674 parameters uncertainty.



675
 676 Figure. 10 Parameters sensitivity analysis for (a) soil moisture content, (b)
 677 groundwater depth, (c) salt salinity concentration, (d) LAI, (e) ET
 678

679 4.4 Model calibration and validation [with field data](#)

680 The model parameters were calibrated and validated using the observed moisture

681 contents, groundwater depth, plant height, leaf area index and the calculated
682 evapotranspiration. For calibration, the data collected in 2017 were used for
683 sunflower fields B and C and maize field A. Since farmers did not grow maize in 2018,
684 the 2017 data of maize field D, together with sunflower fields B and C in 2018 were
685 used for validation. The optimal parameter set was determined using graphical
686 similarity between observed and predicted results together with near optimum
687 performance of the statistical indicators while keeping all values within physical
688 acceptable ranges.

689 As a way of reducing the number of parameters that needed to be calibrated, we
690 initially selected one to three most sensitive parameters for each of the observed time
691 series, starting with evapotranspiration (including LAI and crop height) followed by
692 moisture content, groundwater depth, and salt content in the soil. This cycle was
693 repeated several times until changes became small. The last stage of the calibration
694 consisted of fine-tuning the remaining least sensitive parameters.

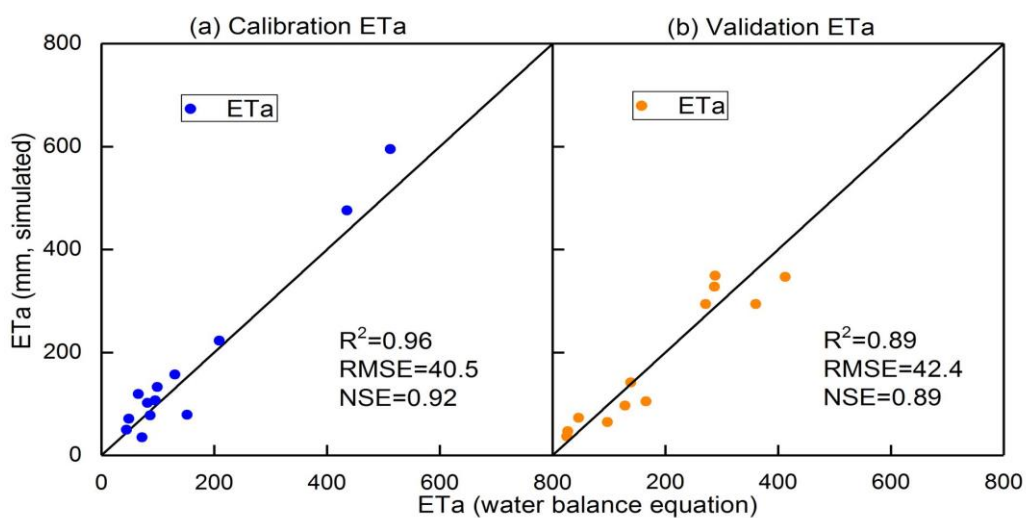
695 To calibrate the parameters in the CROP module, we calculated
696 evapotranspiration during the crop growth period with the observed soil moisture
697 content and groundwater depth by the soil water balance method. In addition, we
698 used the observed LAI measurements in 2017 and plant height in both 2017 and
699 2018. LAI was not measured in 2018. The $DLAI$, LAI_{mx} and H_{mx} in the crop module
700 were adjusted to fit the observed LAI and crop height values. In addition, we fitted the
701 θ_{fc} moisture content to obtain a good fit of the evapotranspiration. The saturated
702 moisture content values were not adjusted since they were already determined for

703 fitting the soil characteristic curve. The exponent b and constant a in Eq. 23 were
704 adjusted to fit the observed soil moisture content and groundwater depth.

705

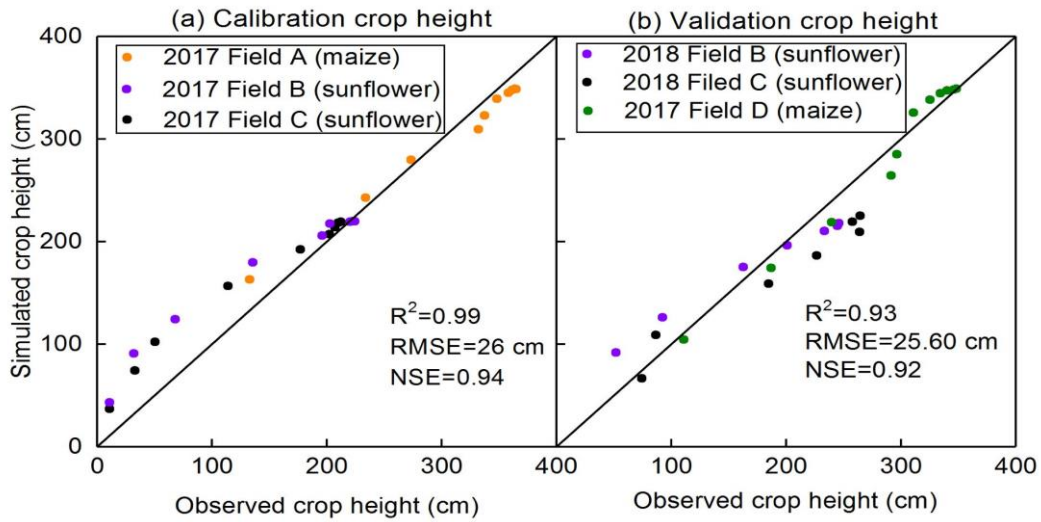
706 4.4.1 Evapotranspiration, crop height and leaf area index

707 The predicted evapotranspiration and that calculated from the mass balance
708 show a good agreement with Nash Sutcliff values ranging from 0.96-0.89 during
709 calibration and validation (Fig. 11 and Table 4). The calibrated predictions of plant
710 height fitted the observed values well during calibration and validation with Nash
711 Sutcliff values ranging from 0.77-0.96 for the individual fields (Table 4) and over 90%
712 when the data was pooled for the fields during calibration and validation (Fig.12). LAI
713 was not measured in 2018. During calibration, Nash Sutcliff predicted LAI values
714 were good for sunflower but not as good for maize but the coefficient of determination
715 and slope in the regression were acceptable (Table 4, Fig. 13). In addition, the overall
716 trend was predicted reasonably well (Fig. 13b).



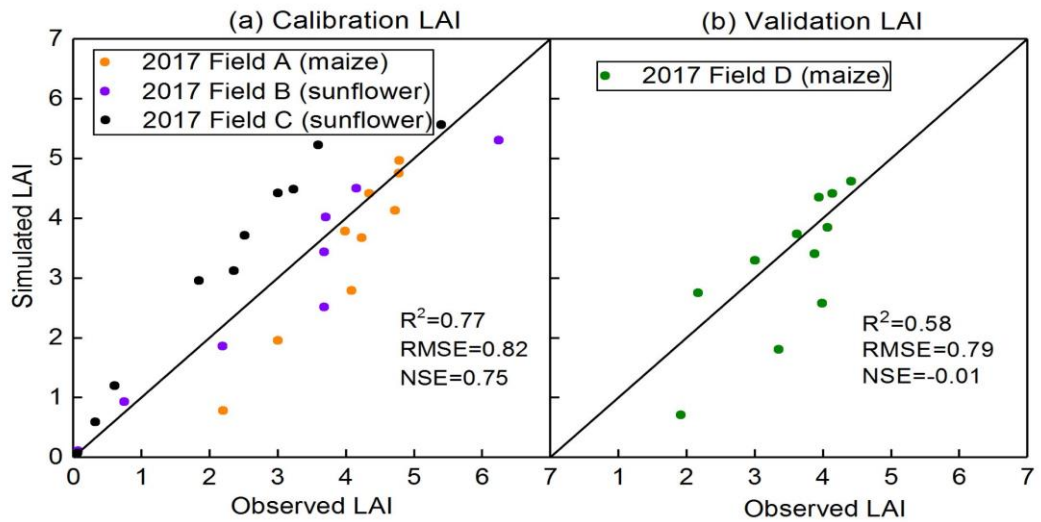
717

718 Fig. 11 Comparison of predicted and observed actual evapotranspiration: a)
719 Calibration and b) Validation



720
721
722
723

Fig.12 Comparison of predicted and observed crop height: a) Calibration and b) Validation



724
725
726
727
728
729
730
731

Fig. 13 Comparison of predicted and observed LAI: a) Calibration and b) validation

732 Table 4 Model error statistics for calibration and validation of model in 2017 and 2018
 733 (Mean relative error, MRE; root mean square error, RMSE; Regression slope;
 734 Coefficient of determination, R²; Regression coefficient, slope).

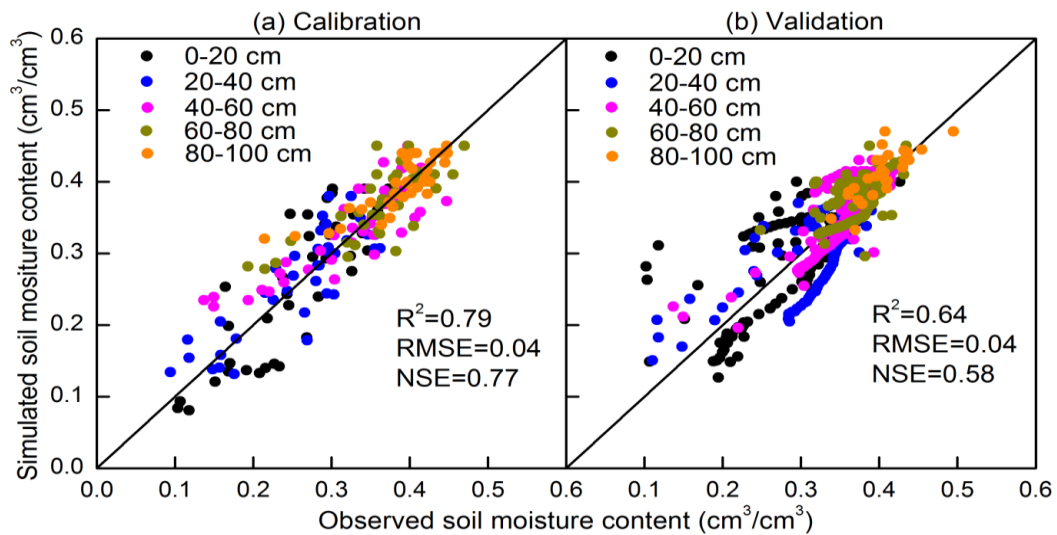
Process	Field	Variable	MRE (%)	RMSE (cm ³ cm ⁻³ cm or gL ⁻¹ or mm)	NSE	R ²	Regression coefficient slope
Calibration	2017 Field A (maize)	SWC (0-1m)	2.9	0.04	0.8	0.56	1.01
		GWD	4.5	33.8	0.64	0.64	0.97
		LAI	-17.4	0.78	0.11	0.92	0.89
		hcrop	0.04	16.2	0.95	0.99	0.97
		C (0-1m)	13.9	0.5	*	0.49	1.07
	2017 Field B (sunflower)	SWC (0-1m)	-1.2	0.04	0.71	0.74	0.97
		GWD	6.0	22.9	0.86	0.98	0.96
		LAI	4.7	0.58	0.9	0.92	0.91
		hcrop	6.8	33.5	0.83	0.96	1.1
		C (0-1m)	11.0	0.55	*	0.7	1.1
	2017 Field C (sunflower)	SWC (0-1m)	8.5	0.04	0.88	0.9	1.05
		GWD	-7.3	19.1	0.91	0.94	0.94
		LAI	48.6	1.0	0.59	0.93	1.29
		hcrop	5.42	27.4	0.88	0.98	1.07
		C (0-1m)	-1.6	0.52	*	0.08	0.94
Validation	2018 Field B (sunflower)	ETa	12.2	40.5	0.92	0.96	1.11
		SWC (0-1m)	-2.3	0.03	0.43	0.68	0.98
		GWD	4.86	16.1	0.83	0.84	1.01
		hcrop	12.5	26.9	0.86	0.99	0.95
	2018 Field C (sunflower)	C (0-1m)	4.0	0.35	*	0.72	1.06
		SWC (0-1m)	17.3	0.06	0.64	0.72	1.04
		GWD	2.1	13.8	0.86	0.87	1.01
		hcrop	-10.3	36.4	0.77	0.97	0.84
		C (0-1m)	0.51	0.33	*	0.73	1.02
	2017 Field D (maize)	SWC (0-1m)	6.1	0.04	0.68	0.77	1.05
		GWD	0.64	39.1	0.52	0.71	1.01
		LAI	-10.7	0.79	-0.02	0.58	0.93
		hcrop	-1.7	13.6	0.96	0.98	1
		C (0-1m)	9.8	0.51	*	0.54	1.11
	ETa	8.0	42.4	0.89	0.89	0.95	

735 Note: * Relative bias was over 5% invalidating the calculation of NSE. SWC is the soil
 736 moisture content, GWD is the groundwater depth, LAI is the leaf area index, hcrop is
 737 the height of the crop, C is the soil salinity concentration, ETa is the actual
 738 evapotranspiration.

739 *4.4.2 Soil moisture and groundwater depth*

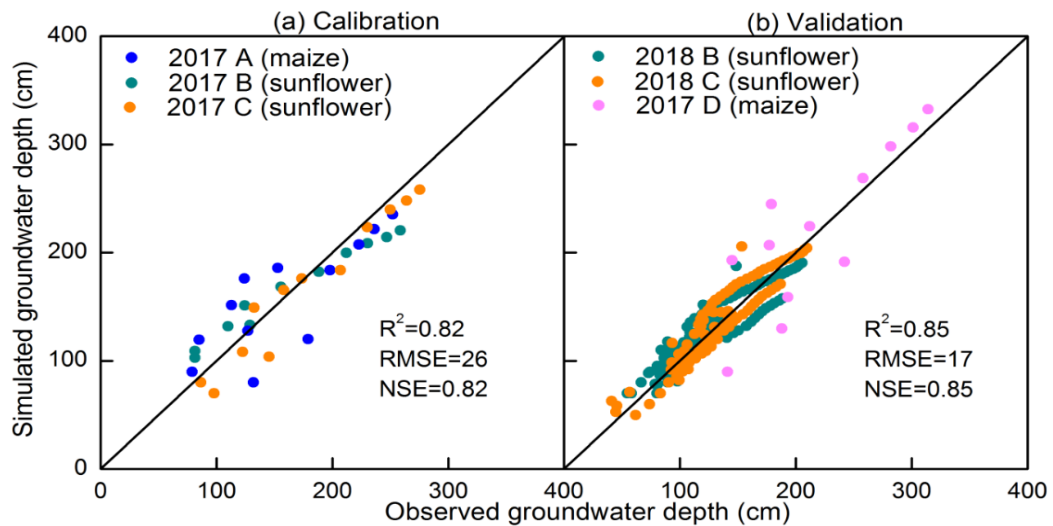
740 Next, the moisture contents and groundwater table were fitted with the parameters in
741 the Vadose model without changing the parameters in the CROP module. Saturated
742 moisture content was the most sensitive parameter for calibrating the moisture
743 content (Fig.10a). Since this value was already determined a priori from the soil
744 characteristic curve (Table 3a), we could not use other parameters to obtain a better
745 fit since none were sensitive (Fig.10a). Therefore, we calibrated the groundwater
746 parameters (i.e., a and b parameters (Eq. 23)) together with the moisture content to
747 obtain the best fit for both. The fitted a and b values are listed in Table 3b. The fitted
748 parameters between the four experimental fields were similar but not the same. This
749 can be expected in river plains where soils can vary over short distances.

750 Overall, the moisture contents were predicted well during calibration and
751 validation (Figs. 5, 14 and Table 4) with the exception of field B during validation
752 (Table 4) with a NSE of 0.43. The moisture contents were predicted most accurately
753 in the layers from 40-100cm where the soil moistures were at field capacity during
754 most of the growing season (Fig. 14). In the top 40 cm, the predicted soil moisture
755 content deviated from observed moisture contents, especially at the dryer end (Fig. 5
756 and 14). Unlike at deeper depths, evapotranspiration determined the moisture
757 contents at shallow depths. Prediction of evapotranspiration introduced additional
758 uncertainties such as the distribution of the root system. This uncertainty is also likely
759 the reason why the 2018 moisture contents during the validation are acceptable but
760 not predicted as well as in 2017.



761
 762 Fig. 14 Comparison of predicted and observed soil moisture content: a) calibration
 763 and b) validation
 764

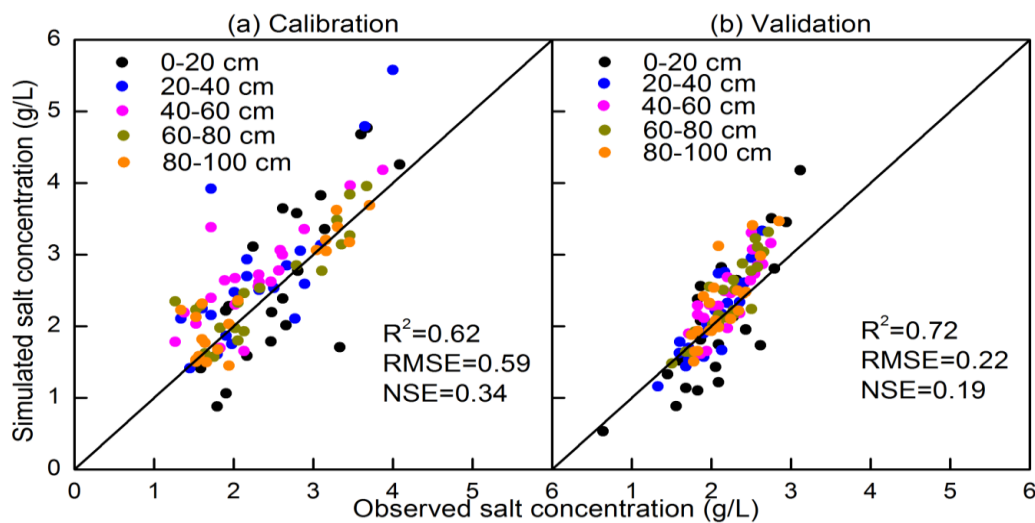
765 The predicted and observed groundwater depths are in good agreement during
 766 both calibration and validation (Figs 7, 15). The MRE values were within $\pm 10\%$ and
 767 the NSE values ranged from 0.52 for field D during validation to 0.91 in field C during
 768 calibration where some of the recharge events were estimated (Table 4).



769
 770 Fig. 15 Comparison of predicted and observed groundwater depth a) calibration and
 771 b) validation.

772 4.4.3 Soil salinity

773 The only parameter that could be adjusted each year for calibration of the salt
774 concentrations was the initial salt concentration. The predicted salt concentrations in
775 the top layers decreased after an irrigation event similar to the limited observed values
776 (Figs. 6). Despite that the salt concentration fitted visually reasonably well as shown in
777 Figures 6 and 16, there was a bias of 8% in the data and consequently the Nash
778 Sutcliff efficiency could not be applied (Table 4) (Ritter and Muñoz-Carpena, 2013).
779 Similarly to the moisture contents, the salt concentrations in the layers below 40 cm
780 were predicted more accurately than the layers above the 40 cm. More data should be
781 collected during the whole year on the salt concentrations in the soil in order to
782 accurately predict the salt concentrations.



783
784 Fig. 16 Comparison of predicted and observed salt concentration during calibration (a)
785 and validation (b)

786 5. Discussion

787 The EPICS model is a surrogate model that can be applied in areas with shallow
788 groundwater. It can simulate the soil moisture content and salt concentration for
789 layers in the soil, the groundwater depth, upward movement of water from

790 groundwater, evapotranspiration, and plant growth.

791 The model is different from traditional models that are based on Richards
792 equation; instead of calculating the fluxes first, in the EPICS model, the groundwater
793 depth is calculated first based either on the amount of water removed by
794 evapotranspiration on days without rain or irrigation or recharge to groundwater on
795 the other days. Subsequently, when the groundwater is sufficiently shallow and the
796 potential upward flux from the groundwater is greater than the evaporative demand,
797 the moisture contents are adjusted so that soil moisture and groundwater depth are in
798 equilibrium (i.e., field capacity). In this case, the matric potential is equal to the height
799 above the water table and the moisture contents can be found with the soil
800 characteristic curve. When the upward flux is less than the evaporative demand of the
801 atmosphere and crop, the difference between the upward moisture content is
802 determined by first decreasing the moisture content below the field capacity. The flux
803 of water in the soil is then calculated based on the changes in water content. The
804 advantage is fewer input parameters needed when compared with other numerical
805 models (Šimůnek et al., 1996; Dam et al., 1997). For example, the hydraulic
806 conductivity is not used in EPICS.

807 Although the uncertainties of field experimental observations and input data of
808 the model affected the accuracy of simulation results, EPICS compares well with
809 other models. Xu et al. (2015) tested the SWAP-EPIC for two lysimeters grown with
810 maize on the same experimental farm in the Hetao irrigation district where our
811 experiment was carried out. The SWAP model solves the Richards' Equation

812 numerically with an implicit backward scheme and is combined by Xu et al. (2015)
813 with the EPIC model. The accuracy of our simulation results, despite the difference in
814 complexity, are very similar. The moisture contents were simulated slightly better with
815 EPICS, the groundwater depth was nearly the same, and the LAI values were
816 predicted more accurately in the SWAP-EPIC model. Xue et al. (2015) did not
817 simulate the salt content of the soil. Compared to less data and computational
818 intensive models that are applied in the Yellow River, the soil moisture content were
819 simulated more accurately by EPICS than in the North China Plain with 30 m deep
820 groundwater by surrogate models of Kendy et al. (2003) and Yang et al. (2015 a,b)
821 and in the Hetao irrigation district by Gao et al. (2017b) and Xue et al. (2018) during
822 the crop growth period.

823 To obtain more accurate results in the future, the upward capillary flux from
824 groundwater needs to be improved. In addition, the evapotranspiration measured
825 independently, using Eddy covariance (Zhang et al., 2012; Armstrong et al., 2008)
826 and Bowen ratio-energy balance method (Zhang et al., 2007) should be further used
827 to test performance of the model in the future study.

828 The limitation of the EPICS model is it can only be applied in areas where
829 groundwater is generally less than 3.3 m deep. When the groundwater is deeper than
830 3.3 m, the field capacity of the surface soil is determined by the moisture content
831 when the hydraulic conductivity becomes limiting and not by the depth of the
832 groundwater.

833 Overall, the present model has the advantage that it greatly simplifies the

834 calculation of the moisture content, groundwater depth and salt content and despite
835 that, gives results similar to or better than other models applied in the Yellow river
836 basin.

837 **6. Conclusions**

838 A novel surrogate field hydrological model called *Evaluation of the Performance*
839 *of Irrigated Crops and Soils* (EPICS) was developed for irrigated areas with shallow
840 groundwater. The model was tested with two years experimental data collected by us
841 for sunflower and one year of maize on replicated fields in the Hetao irrigation district,
842 a typical arid to semi-arid irrigation district with a shallow aquifer. The EPICS model
843 uses the soil moisture characteristic curve, upward capillary flux, and groundwater
844 depth to derive the drainable porosity and predict the soil moisture contents and
845 salinity. The evaporative flux is calculated with equations in EPIC (Environmental
846 Policy Integrated Climate) and root distribution equation.

847 The simulation results show that the EPICS model can predict the soil moisture
848 content and salt concentration in different soil layers, groundwater depth, and crop
849 growth on a daily time step with acceptable accuracy during calibration and validation.
850 The saturated soil moisture content is the most sensitive parameter for soil moisture
851 content, salt concentration, and ET in our model.

852 In the future, the model should be tested in other areas with shallow groundwater
853 that can be found in surface irrigated sites and in humid climates in river plains. Once
854 fully tested, the EPICS model can be used for optimizing water use at the local scale
855 but, more importantly, on a watershed scale in closed basins where every drop of

856 water counts.

857

858 **Data availability:** The observed data used in this study are not publicly accessible.

859 These data have been collected by personnel of the College of Water Resources and

860 Civil Engineering, China Agricultural University, with funds from various cooperative

861 sources. Anyone who would like to use these data, should contact Zhongyi Liu,

862 Xianghao Wang and Zailin Huo to obtain permission.

863 **Author contributions:** LZ and XW collected the data. ZL, ZH, CW, GH, XX and TS

864 contributed to the development of the model. The simulations with the model were

865 done by ZL, ZH and TS. Preparation and revision of the paper were done by ZL under

866 the supervision of TS and ZH.

867 **Competing interests:** The authors declare that they have no conflicts of interest.

868 **Acknowledgements:** Peggy Stevens helped greatly with polishing the English. We

869 thank Xianghao Wang and Limin Zhang and the technicians in the Shahaqu

870 experimental station who helped in collecting data.

871 **Financial support:** This study has been supported by National Key Research and

872 Development Program of China (2017YFC0403301) and the National Natural

873 Science Foundation of China (No. 51639009, 51679236).

874

875

876

877

- 879 Abrahart, R.J and See, L.: Comparing neural network and autoregressive moving
880 average techniques for the provision of continuous river flow forecasts in two
881 contrasting catchments. *Hydro. Processes*, 14: 2157-2172. [http://doi.org/10.1002/1099-1085\(20000815/30\)14:11/12<2157::AID-HYP57>3.0.CO;2](http://doi.org/10.1002/1099-1085(20000815/30)14:11/12<2157::AID-HYP57>3.0.CO;2-S)
882 -S. 2000.
883
- 884 Allen, R.G., Pereira, L.S., Raes, D., and Smith, M.: Crop evapotranspiration.
885 Guidelines for computing crop water requirements-FAO Irrigation and Drainage
886 Paper 56, FAO, Rome. 1998
- 887 Armstrong, R.N., Pomeroy, J. W., Martz, L.W.: Evaluation of three evaporation
888 estimation methods in a Canadian prairie landscape. *Hydrol. Process*, 22(5):
889 2801-2815. <https://doi.org/10.1002/hyp.7054>. 2008.
- 890 Asher, M.J., Croke, B.F.W., Jakeman, A.J. and Peeters, L.J.M.: A review of surrogate
891 models and their application to groundwater modeling. *Water Resour Res*,
892 51:5957-5973. <http://doi.wiley.com/10.1002/2015WR016967>. 2015. Blanning, R.
893 W., The construction and implementation of metamodels, *Simulation*, 24(6):
894 177-184. <https://doi.org/10.1177/003754977502400606>. 1975.
- 895 Babajimopoulos, C., Panoras, A., Georgoussis, H., Arampatzis, G., Hatzigiannakis, E.,
896 Papamichail, D.: Contribution to irrigation from shallow water table under field
897 conditions. *Agr. Water Manage.* 92:2015-210. <https://doi.org/10.1016/j.agwat.2007.05.009>
898
- 899
- 900 Brooks, R.H., and Corey, A.T.: Hydraulic properties of porous media, Hydrology
901 Paper 3. Colorado State University. Fort Collins, Colorado, 37pp, 1964.
- 902 Blanning, R.W.: Construction and Implementation of Metamodels. *Simulation*,
903 24(6):177-184. <https://doi.org/10.1177/003754977502400606>. 1975.
- 904 Chen, C., Wang, E., and Yu, Q.: Modelling the effects of climate variability and water
905 management on crop water productivity and water balance in the North China
906 Plain. *Agr. Water Manage.*, 97:1175-1184. <https://doi.org/10.1016/j.agwat.2008.11.012>. 2010.
907
- 908 Chen, S., Huo, Z., Xu, X., Huang, G.: A conceptual agricultural water productivity
909 model considering under field capacity soil water redistribution applicable for arid
910 and semi-arid areas with deep groundwater, *Agr Water Manage*, 213, 309-323.
911 <https://doi.org/10.1016/j.agwat.2018.10.024>. 2019.

- 912 Cloke, H., Pappenberger, F., Renaud, J.: Multi-Method Global Sensitivity Analysis
913 (MMGSA) for modelling floodplain hydrological processes. *Hydrol Process*, 22(1):
914 1660-1674. [https:// doi.org/ 10.1002/hyp.6734](https://doi.org/10.1002/hyp.6734). 2008.
- 915 Cuo, L., Giambelluca, T., Ziegler, A.: Lumped parameter sensitivity analysis of a
916 distributed hydrological model within tropical and temperate catchments. *Hydrol*
917 *Process*, 25(15): 2405-2421. [http://doi.org/ 10.1002/hyp.8017](http://doi.org/10.1002/hyp.8017). 2011.
- 918 Dam, J.C. Van., Huygen, J., Wesseling, J.G., Feddes, R.A., Kabat, P., Walsum, P.E.V.
919 Van., Groenendijk, P., Diepen.: Theory of SWAP version 2.0. Simulation of water
920 flow, solute transport and plant growth in the soil-water-atmosphere-plant
921 environment. Report 71, Department Water Resources, Wageningen Agricultural
922 University. Technical document 45, DLO Winand Staring Centre,
923 Wageningen, 152pp, 1997.
- 924 Dawson, C.W., Abrahart, R.J., Shamseldin, A.Y., Wilby, R.L.: Flood estimation at
925 ungauged sites using artificial neural networks. *J Hydrol.* 319: 391-409.
926 [http://doi.org/10.1016/ .jhydrol.2005.07.032](http://doi.org/10.1016/j.jhydrol.2005.07.032). 2006.
- 927 Dehaan, R., and Taylor, G.: Field-derived spectra of salinized soils and vegetation as
928 indicators of irrigation-induced soil salinization, *Remote Sens Environ*, 80(3),
929 406-417. [https:// doi.org/10.1016/S0034-4257\(01\)00321-2](https://doi.org/10.1016/S0034-4257(01)00321-2). 2002.
- 930 Delongue, K. C., Ascough, J. C., Andales, A. A., Hansen, N. C., Garcia, L. A., Arabi, M.:
931 Improving evapotranspiration simulations in the CERES-Maize model under
932 limited irrigation. *Agr Water Manage*, 115: 92-103. [http://doi.org/](http://doi.org/10.1016/j.agwat.2012.08.013)
933 [10.1016/j.agwat.2012.08.013](http://doi.org/10.1016/j.agwat.2012.08.013). 2012.
- 934 Doherty, J. and Simmons C.: Groundwater modelling in decision support: reflections
935 on a unified conceptual framework, *Hydrogeol. J*, 21(7), 1531-1537. [https://](https://doi.org/10.1007/s10040-013-1027-7)
936 doi.org/10.1007/s10040-013-1027-7. 2013.
- 937 Feng, Z., Wang, X., Feng, Z.: Soil N and salinity leaching after the autumn irrigation
938 and its impact on groundwater in Hetao Irrigation District, China. *Agr Water*
939 *Manage*, 71(2): 131-143. [https:// doi.org/10.1016/j.agwat.2004.07.001](https://doi.org/10.1016/j.agwat.2004.07.001). 2005.
- 940 Flint, A.L., Flint, L.E., Kwicklis, E.M., Fabryka-Martin, J.T., and Bodvarsson, G.S.:
941 Estimating recharge at Yucca Mountain, Nevada, USA: comparison of methods.
942 *Hydrogeol. J.*, 10:180-204. [https:// doi.org/ 10.1007/s10040-001-0169-1](https://doi.org/10.1007/s10040-001-0169-1). 2002.

943 Gao, X., Huo, Z., Bai, Y., Feng, S., Huang, G., Shi, H., and Qu, Z.: Soil salt and
944 groundwater change in flood irrigation field and uncultivated land: a case study
945 based on 4-year field observations. *Environ. Earth Sci.*, 73:2127-2139. <https://doi.org/10.1007/s12665-014-3563-4>. 2015.

947 Gao, X., Huo, Z., Qu, Z., Xu, X., Huang, G., and Steenhuis, T.S.: Modeling
948 contribution of shallow groundwater to evapotranspiration and yield of maize in
949 an arid area. *Sci. Rep-UK* 7. <https://doi.org/10.1038/srep43122>. 2017.

950 Gardner, W.: Some steady-state solutions of the unsaturated moisture flow equation
951 with application to evaporation from a water table. *Soil Sci.*, 85:228-232. 1958.

952 Gardner, W., Hillel, D., and Benyamini, Y.: Post-Irrigation Movement Soil Water 1.
953 Redistribution. *Water Resour Res.*, 6:851-860. <https://doi.org/10.1029/WR006i003p00851>. 1970a.

955 Gardner, W., Hillel, D., and Benyamini, Y.: Post-Irrigation Movement of Soil Water 2.
956 Simultaneous Redistribution and Evaporation. *Water Resour Res.*, 6:1148-1153.
957 <https://doi.org/10.1029/WR006i004p01148>. 1970b.

958 Guo, S., Ruan, B., Chen, H., Guan, X., Wang, S., Xu, N. and Li, Y.: Characterizing the
959 spatiotemporal evolution of soil salinization in Hetao Irrigation District (China)
960 using a remote sensing approach. *Int J Remote Sens* 39: 6805-6825. <https://doi.org/10.1080/01431161.2018.1466076>. 2018.

962 [Hanson, B., Hopmans, J., Šimůnek, J.: Leaching with Subsurface Drip Irrigation
963 under Saline, Shallow Groundwater Conditions. *Vadose Zone J.* 7, 810-818.
964 <http://doi.org/10.2136/vzj2007.00532008>. 2008.](http://doi.org/10.2136/vzj2007.00532008)

965 Hsiao, T., Heng, L., Steduto, P., Rojas-Lara, B., Raes, D., Fereres, E.: AquaCrop-The
966 FAO Crop Model to Simulate Yield Response to Water: III. Parameterization and
967 Testing for Maize. *Agron. J.*, 101(3):448-459. <https://doi.org/10.2134/agronj2008.0218s>. 2009.

969 Hu, S., Shi, L., Huang, K., Zha, Y., Hu, X., Ye, H., Yang, Q.: Improvement of
970 sugarcane crop simulation by SWAP-WOFOST model via data assimilation.
971 *Field Crop Res.*, 232: 49-61. <https://doi.org/10.1016/j.fcr.2018.12.009>. 2019.

972 Huang, Q., Xu, X., Lu, L., Ren, D., Ke, J., Xiong, Y., Huo, Z. and Huang, G.: Soil
973 salinity distribution based on remote sensing and its effect on crop growth in

- 974 Hetao Irrigation District. Transactions of the Chinese Society of Agricultural
975 Engineering, 34:102-109. 2018.
- 976 Kendy, E., Gérard-Marchant, P., Walter, M. T., Zhang, Y., Liu, C., and Steenhuis, T.S.:
977 A soil-water-balance approach to quantify groundwater recharge from irrigated
978 cropland in the North China Plain. Hydrol. Process., 17:2011-2031. <https://doi.org/10.1002/hyp.1240>. 2003.
- 980 Leube, P. C., : Temporal moments revisited: Why there is no better way for physically
981 based model reduction in time, Water Resour Res, 48(11): W11527. <https://doi.org/10.1029/2012WR011973> 2012.
- 983 Li, J., Pu, L., Han, M., Zhu, M., Zhang, R., Xiang, Y.: Soil salinization research in
984 China: Advances and prospects, J Geogr Sci, 24(5), 943-960. <https://doi.org/10.1007/s11442-014-1130-2> .2014
- 986 [Letey, J., Hoffman, G.J., Hopmans, J.W., Grattan, S.R., Suarez, D., Corwin, D.L.,](#)
987 [Oster, J.D., Wu, L., Amrhein, C.: Evaluation of soil salinity leaching requirement](#)
988 [guidelines. Agric. Water Manag. 98, 502–506.](#)
989 <https://doi.org/10.1016/j.agwat.2010.08.009>. 2011.
- 990 Li, X., Zhao, Y., Xiao, W., Yang, M., Shen, Y., Min, L.: Soil moisture dynamics and
991 implications for irrigation of farmland with a deep groundwater table. Agr. Water
992 Manage.,192:138-148. <https://doi.org/10.1016/j.agwat.2017.07.003>.2017.
- 993 Liu, J.: A GIS-based tool for modelling large-scale crop-water relations. Environ
994 Modell Softw. 24(3): 411-422. <https://doi.org/10.1016/j.envsoft.2008.08.004>.
995 2009.
- 996 Liu, Z., Wang, X., Huo, Z, Steenhuis, T.S.: A unique vadose zone model for shallow
997 aquifers: the Hetao irrigation district, China. Hydrol Earth Syst Sc.
998 23(7):3097-3115. <https://doi.org/10.5194/hess-23-3097-2019>. 2019.
- 999 Luo, Y., and Sophocleous, M.: Seasonal groundwater contribution to crop-water use
1000 assessed with lysimeter observations and model simulations. J. Hydrol,
1001 389:325-335. <https://doi.org/10.1016/j.jhydrol.2010.06.011>. 2010.
- 1002 Ma, Y., Feng, S., and Song, X.: A root zone model for estimating soil water balance
1003 and crop yield responsesto deficit irrigation in the North China Plain. Agr. Water
1004 Manage., 127:13-24. <https://doi.org/10.1016/j.agwat.2013.05.011>. 2013.

- 1005 Miao, Q., Rosa, R., Shi, H., Paredes, P., Zhu, L., Dai, J., Goncalves, J., Pereira, L.:
1006 Modeling water use, transpiration and soil evaporation of spring wheat–maize
1007 and spring wheat–sunflower relay intercropping using the dual crop coefficient
1008 approach. *Agr Water Manage*, 165:211-229.
1009 <https://doi.org/10.1016/j.agwat.2015.10.024.2016>.
- 1010 Minhas, P., Ramos, T., Ben-Gal., A., Pereira, L.: Coping with salinity in irrigated
1011 agriculture: Crop evapotranspiration and water management issues. *Agr Water*
1012 *Manage*, 227, 105832. <https://doi.org/10.1016/j.agwat.2019.105832>. 2020.
- 1013 Moriasi, D. N., Arnold, J. G., Van Liew, M. W., Bingner, R. L., Harmel, R. D., Veith, T.
1014 L.: Model evaluation guidelines for systematic quantification of accuracy in
1015 watershed simulations. *T ASABE*, 50(3): 885-900. 2007.
- 1016 Nash, J.E., and Sutcliffe, J.V.: River flow forecasting through conceptual models part I
1017 – a discussion of principles. *J Hydrol*. 10:282-290. 1970.
- 1018 Novark, V.: Estimation of Soil-water Extraction Patterns by Roots, *Agr Water Manage*,
1019 12(4), 271-278. [https://doi.org/10.1016/0378-3774\(87\)90002-3](https://doi.org/10.1016/0378-3774(87)90002-3). 1987
- 1020 Phogat, V., Mallants, D., Cox, J., Šimůnek, J., Oliver, D., Awad, J.: Management of
1021 soil salinity associated with irrigation of protected crops. *Agr. Water Mange.*,
1022 227:105845. <https://doi.org/10.1016/j.agwat.2019.105845.2020>.
- 1023 Raes, D., Steduto, P., Hsiao, T., Fereres.: AquaCrop-The FAO Crop Model to
1024 Simulate Yield Response to Water: II. Main Algorithms and Software Description,
1025 *Agron. J*, 101(3), 438. <https://doi.org/10.2134/agronj2008.0140s.2009>.
- 1026 Regis, R., and Shoemaker, C.: Constrained Global Optimization of Expensive Black
1027 Box Functions Using Radial Basis Functions, *J Global Optim*, 31(1), 153-171.
1028 <https://doi.org/10.1007/s10898-004-0570-0>. 2005.
- 1029 Ren, D., Xu, X., Hao, Y., and Huang, G.: Modeling and assessing field irrigation water
1030 use in a canal system of Hetao, upper Yellow River basin: Application to maize,
1031 sunflower and watermelon. *J. Hydrol*, 532:122-139. <https://doi.org/10.1016/j.jhydrol.2015.11.040>. 2016.
- 1033 Ren, D., Xu, X., Romos, T., Huang, Q., Huo, Z., Huang, G.: Modeling and assessing
1034 the function and sustainability of natural patches in salt-affected
1035 agro-ecosystems: Application to tamarisk (*Tamarix chinensis* Lour.) in Hetao,
1036 upper Yellow River basin. *J. Hydrology*.

- 1037 [532:490-504.https://doi.org/10.1016/j.jhydrol.2017.04.054.2017.](https://doi.org/10.1016/j.jhydrol.2017.04.054.2017)
- 1038 Rengasamy, P.: World salinization with emphasis on Australia, *J Exp. Bot.*, 57(5),
1039 1017-1023. [https:// doi.org/10.1093/jxb/erj108](https://doi.org/10.1093/jxb/erj108) .2006
- 1040 Rhoades, J., Manteghi, N., Shouse, P., Alves, W.: Soil Electrical Conductivity and
1041 Soil Salinity: New Formulations and Calibrations, *Soil Sci. Soc. Am. J.*, 53(2):
1042 433-439. [https:// doi.org/ 10.2136/sssaj1989.03615995005300020020x](https://doi.org/10.2136/sssaj1989.03615995005300020020x). 1989.
- 1043 Ritter, A., and Muñoz-Carpena, R.: Performance evaluation of hydrological models:
1044 Statistical significance for reducing subjectivity in goodness-of-fit assessments. *J*
1045 *Hydrol.*, 480:33-45. 2013.[http:// doi.org/ 10.1016/j.jhydrol.2012.12. 004](http://doi.org/10.1016/j.jhydrol.2012.12.004). 2013.
- 1046 Rosa, R.D., Paredes, P., Rodrigues, G.C., Alves, I, Fernando, R.M., Pereira, L.S.,
1047 Allen, R.G.: Implementing the dual crop coefficient approach in interactive
1048 software. 1. Background and computational strategy. *Agr. Water Manage.*, 103:
1049 8-24. [https:// doi.org/10.1016/j.agwat.2011.10.013](https://doi.org/10.1016/j.agwat.2011.10.013). 2012.
- 1050 Sau, F., Boote, K., Bostick, W., Jones, J., Minguéz, M.,: Testing and improving
1051 evapotranspiration and soil water balance of the DSSAT crop models. *Agron. J.*,
1052 96: 1243-1257. [https:// doi.org/ 10.2134/agronj2004.1243](https://doi.org/10.2134/agronj2004.1243). 2004.
- 1053 Shelia, V., Simunek, J., Boote, K., Hoogenboom, G.: Coupling DSSAT and
1054 HYDRUS-1D for simulations of soil water dynamics in the soil-plant-atmosphere
1055 system. *J Hydrol Hydromech.*, 66(2): 232-245. [https://](https://doi.org/10.1515/johh-2017-0055)
1056 doi.org/10.1515/johh-2017-0055. 2018.
- 1057 Šimunek, J., Šejna, M. and van Genuchten, M.T.: The HYDRUS-1D software
1058 package for simulating the one-dimensional movement of water, heat, and
1059 multiple solutes in variably-saturated media. Version 2.0. IGWMC-TPS-70. Int.
1060 Groundwater Modeling Ctr., Colorado School of Mines, Golden. 1998.
- 1061 Steduto, P., Hsiao, T., Raes, D., Fereres, E.: AquaCrop-The FAO Crop Model to
1062 Simulate Yield Response to Water: I. Concepts and Underlying Principles. *Agron*
1063 *J.*, 101(3):426-437. [https:// doi.org/10.2134/agronj2008.0139s](https://doi.org/10.2134/agronj2008.0139s). 2009.
- 1064 Steenhuis, T., Richard, T., Parlange, M., Aburime, S., Geohring, L., Parlange, J.:
1065 Preferential Flow Influences on Drainage of Shallow Sloping Soils. *Agr Water*
1066 *Manage.*, 14(1-4):137-151. [https:// doi.org/ 10.1016/0378-3774\(88\)90069-8](https://doi.org/10.1016/0378-3774(88)90069-8).
1067 1988.

- 1068 Uehara, G.: Technology-transfer in the tropics. *Outlook Agr.*, 18(1): 38-42. <https://doi.org/10.1177/003072708901800107>. 1989.
- 1069
- 1070 Van Diepen, C., Wolf, J., van Keulen, H., Rappoldt, C.: WOFOST A STIMULATION
1071 MODEL OF CROP PRODUCTION. *Soil Use and Management*, 5(1): 16-24.
1072 1989.
- 1073 Wallender, W. , Tanji, K. : Agricultural salinity assessment and management.
1074 Agricultural salinity assessment and management. Ed.2. American Society of
1075 Civil Engineers (ASCE), Reston, USA. University of California-Davis, USA.:
1076 xxx+1094pp. 2011.
- 1077 Wang, X., Huang, G., Yang, J., Huang, Q., Liu, H., Yu, L.: An assessment of irrigation
1078 practices: Sprinkler irrigation of winter wheat in the North China Plain. *Agr Water*
1079 *Manage.*, 159: 197-208. [https:// doi.org/ 10.1016/j.agwat.2015.06.011](https://doi.org/10.1016/j.agwat.2015.06.011). 2015.
- 1080 Wang, J., Huang, G., Zhan, H., Mohanty, B., Zheng, J., Huang, Q., Xu, X.: Evaluation
1081 of soil water dynamics and crop yield under furrow irrigation with a
1082 two-dimensional flow and crop growth coupled model. *Agr Water Manage.*, 141:
1083 10-22. [https:// doi.org /10.1016/j.agwat.2014.04.007](https://doi.org/10.1016/j.agwat.2014.04.007). 2014.
- 1084 [Wu, X., Zheng, Y., Wu, B., Tian, Y., Han, F., Zheng, C.: Optimizing conjunctive use of](#)
1085 [surface water and groundwater for irrigation to address human-nature water](#)
1086 [conflicts: A surrogate modeling approach. *Agr Water Manage*, 163\(1\): 380-392.](#)
1087 [https:// doi.org/10.1016/j.agwat.2015.08.022](https://doi.org/10.1016/j.agwat.2015.08.022). 2016.
- 1088 Williams, J., Jones, C., Kiniry, J., and Spanel, D.: The EPIC Crop Growth Model. *T.*
1089 *ASAE*, 32:479-511. 1989.
- 1090 Williams, W. D., Salinisation: A major threat to water resources in the arid and
1091 semi-arid regions of the world, *Lakes Reservoirs Research and Management*,
1092 4(3-4), 85-91. [https:// doi.org/10.1046/j.1440-1770.1999.00089.x](https://doi.org/10.1046/j.1440-1770.1999.00089.x). 1999.
- 1093 Willcox, K., and Peraire J.: Balanced Model Reduction via the Proper Orthogonal
1094 Decomposition, *AIAA J*, 40(11), 2323-2330. [https:// doi.org/10.2514/2.1570](https://doi.org/10.2514/2.1570).
1095 2002.
- 1096 Xu, X., Sun, C., Qu, Z., Huang, Q., Ramos, T.B., and Huang, G.: Groundwater
1097 Recharge and Capillary Rise in Irrigated Areas of the Upper Yellow River Basin
1098 Assessed by an Agro-Hydrological Model. *Irrig. Drain.*, 64:587-599. <https://doi.org/10.1002/ird.1928>. 2015.
- 1099

- 1100 Xu, X., Sun, C., Huang, G., Mohanty, B.: Global sensitivity analysis and calibration of
1101 parameters for a physically-based agro-hydrological model. *Environ Modell*
1102 *Softw.*, 83: 88-102. [https:// doi.org/10.1016/j.envsoft.2016.05.013](https://doi.org/10.1016/j.envsoft.2016.05.013). 2016.
- 1103 Xu, X., Huang, G., Sun, C., Pereira, L., Ramos, T., Huang, Q., Hao, Y.: Assessing the
1104 effects of water table depth on water use, soil salinity and wheat yield: Searching
1105 for a target depth for irrigated areas in the upper Yellow River basin. *Agr Water*
1106 *Manage*, 125: 46-60. [https:// doi.org/10.1016/j.agwat.2013.04.004](https://doi.org/10.1016/j.agwat.2013.04.004). 2013.
- 1107 Xu, X., Huang, G., Qu, Z., and Pereira, L.S.: Assessing the groundwater dynamics
1108 and impacts of water saving in the Hetao Irrigation District, Yellow River basin.
1109 *Agr Water Manage.*, 98:301-313. [https:// doi.org/10.1016/j.agwat.2010.08.025](https://doi.org/10.1016/j.agwat.2010.08.025).
1110 2010.
- 1111 Xue, J., Huo, Z., Wang, F., Kang, S., and Huang, G.: Untangling the effects of shallow
1112 groundwater and deficit irrigation on irrigation water productivity in arid region:
1113 New conceptual model. *Sci. Total Environ.*, 619-620:1170-1182. [https://](https://doi.org/10.1016/j.scitotenv.2017.11.145)
1114 doi.org/10.1016/j.scitotenv.2017.11.145 2018.
- 1115 Yang, X., Chen, Y., Pacenka, S., Gao, W., Ma, L., Wang, G., Yan, P., Sui, P., and
1116 Steenhuis, T. S.: Effect of diversified crop rotations on groundwater levels and
1117 crop water productivity in the North China Plain, *J. Hydrol.*, 522, 428–438,
1118 <https://doi.org/10.1016/j.jhydrol.2015.01.010>, 2015a.
- 1119 Yang, X., Chen, Y., Pacenka, S., Gao, W., Zhang, M., Sui, P., and Steenhuis, T. S.:
1120 Recharge and groundwater use in the North China Plain for six irrigated crops for
1121 an eleven year period, *Plos One*, 10, e0115269, <http://doi.org/10.1371/journal.pone.0115269>,
1122 [http:// doi.org/10.1371/10.1371/journal.pone.0115269](http://doi.org/10.1371/10.1371/journal.pone.0115269), 2015b.
- 1123 Yeh, P.J., and Famiglietti, J.S.: Regional groundwater evapotranspiration in Illinois. *J.*
1124 *Hydrometeorol.*, 10:464-478. [https:// doi.org/ 10.1175/2008JHM1018.1](https://doi.org/10.1175/2008JHM1018.1). 2009.
- 1125 Zhang, B., Kang, S., Zhang, L., Du, T., Li, S., Yang, X.: Estimation of seasonal crop
1126 water consumption in a vineyard using Bowen ratio-energy balance method.
1127 *Hydrol. Process*, 21(6): 3635-3641. [https:// doi.org/ 10.1002/hyp.6568](https://doi.org/10.1002/hyp.6568).
- 1128 Zhang, F., Zhou, G., Wang, Y., Yang, F., Nilsson, C.: Evapotranspiration and crop
1129 coefficient for a temperate desert steppe ecosystem using eddy covariance in
1130 Inner Mongolia, China. *Hydrol. Process*, 26(3): 379-386. [https:// doi.org/](https://doi.org/10.1002/hyp.8136)
1131 [10.1002/hyp.8136](https://doi.org/10.1002/hyp.8136).